ABSTRACT

Title of Thesis:	Effect of cargo location on translocation of cell-penetrating peptide fusion proteins into *Candida albicans* cells
	Marzyeh Kheradmand-Hajibashi, Master of science, 2021
Thesis Directed By:	Dr. Amy J. Karlsson, Department of Chemical and Biomolecular Engineering

Resistance to antifungal drugs is an increasing issue in treating disease caused by the fungal pathogen *Candida albicans*. As a step towards new antifungal approaches, we investigated antifungal delivery of molecules to *C. albicans* cells using the cell-

penetrating peptide, MPG, genetically fused to the model cargo, green fluorescent protein (GFP). We varied the orientation of the fusion of GFP to MPG and evaluated translocation into the cells. We found fusing the GFP to the C-terminus of the peptide resulted in translocation into almost 5% of C. *albicans* cells, while fusion of GFP to the N-terminus of the peptide resulted in translocation into less than 0.3% of cells. Our results indicate that fusion of cargo to the C-terminus of MPG is preferred for intracellular delivery of cargo, but further research to improve the efficiency of translocation into the cells is required.

Effect of cargo location on translocation of cell-penetrating peptide fusion proteins into *Candid albicans* cells

By

Marzyeh Kheradmand-Hajibashi

Thesis submitted to the Faculty of the Graduate School of the
University of Maryland, College Park, in partial fulfillment
of the requirements for the degree of
Master of science
2021

Advisory Committee:

Dr. Amy J. Karlsson, Chair

Dr. Jeffery B. Klauda

Dr. Ganesh Sriram

Dedication

I wholeheartedly dedicate this thesis to my beloved parents Mr. Mohsen Kheradmand and Mrs. Fatemeh Attaran. Thanks to their endless love, encouragement, and support through this path.

Acknowledgements

Foremost, I would like to express my deepest appreciation to my lovely advisor, Dr. Amy J. Karlsson whose words of advice, patience, and faith made completion of this study possible. Her active engagement and interest in research was my main source of inspiration over the past two years.

I would like to thank our group, especially Dr. Sayanee Adhikari, who helped me get started in the lab. She thought me on every technique required for my experiments and I kept her engaged in the lab with my troubles even after her graduation.

A debt of gratitude is also owed to Shakiba Nikfarjam for being such a wonderful and supportive friend. She is the first one who I run to when I face troubles and she has always been there for me.

I was honored to join the lab simultaneously with two wonderful friends, Dinara Konakbayeva and Wright Makambi who are like my family and made the lab a lovely place to work. Special thanks to Dinara for spending time helping me troubleshoot my experiments and supporting me. And Wright, our fungal expert, thanks for all your supports and distractions.

I would also like to thank Jiwon Wu, who started in the lab as an undergrad and Sayanee trained both of us, but covid limited the time we spent with her, and I really enjoyed doing experiments with her.

I would also like to thank Kenneth Class, for helping with the flow cytometry assay that was impossible without his help.

And finally, especial thanks to my parents, my sister and my brother for supporting me to follow the path that I love.

Table of Contents

List of Tables

List of Figures

List of Abbreviations

CD	Circular dichroism
CPP	Cell-penetrating peptide
DLS	dynamic light scattering
DNA	Deoxyribonucleic acid
DTT	Dithiothreitol
FAM	Carboxyfluorescein
FDA	Food and drug administration
G_4S	Glycine-serine linker
GFP	Green fluorescent protein
HF	High fidelity
HIV	human immunodeficiency virus
HRP	Horse-radish peroxidase
IMAC	Immobilized metal affinity chromatography
IPTG	Isopropyl β-D-1-thiogalactopyranoside
LB	Lysogeny broth
MAP	Multiple Antigenic Peptide
MW	Molecular weight
NaPB	Sodium Phosphate Buffer
NGC	Next generation chromatography
NLS	Nuclear localization sequence
OD	Optical density
PBS	Phosphate-buffered saline

PCR	Polymerase chain reaction
PI	Propidium iodide
RPM	Round per minute
SEC	Size exclusion chromatography
UV	Ultraviolet
YPD	Yeast extract peptone dextrose medium

Chapter 1: Background and motivation

1.1 Fungal infection and Candida albicans

Candida species are the most common human fungal pathogens[1], and the infection caused by these pathogens is called candidiasis. Candidiasis can affect human mucosal surfaces or skin, like vulvovaginal and oropharyngeal candidiasis, or it can cause a systemic, life-threatening infection by invading different organs of the body[1,2].

Candida albicans is the most common species of *Candida* that is collected from patients diagnosed with candidiasis. An important characteristic of *C. albicans* is its ability to grow in two major forms, namely, yeast and hyphal forms (Figure 1.1), making it dimorphic. Studies have shown that the hyphal form has more adherence to organs and tissues, which is required by *C. albicans* for invasion, while the yeast form is responsible for spread of infection[1]. If the hyphal transition is inhibited in *C. albicans*, the yeast form of the cells will still infect tissues and organs, but the severity and lethality of infection was observed to be much less compared to when filamentation of *C. albicans* occurs[1]. The growth conditions are an important factor for the dimorphic transition, with the combination of 37 ℃ and pH=7 being the best physical conditions for hyphal

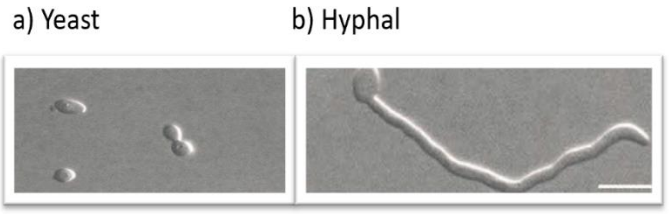

Figure 1.1 The dimorphic switch. *C. albicans* switch from (a) yeast form to (b) hyphal form. The scale bar represents 10 μm. Figure reprinted with permission from Sudbery et al. Copyright 2004 Elsevier Ltd 46.

formation[3]. The nutrients in the growth media are of high importance as well. For example, horse serum was introduced in the media for transition to hyphal form[3].

C. albicans is present as a commensal in the human skin, mouth, gut, vagina, and mucous membranes[1]. It can cause systematic infections when the conditions for growth and proliferation are provided by the environment inside the body of individuals with suppressed immune systems. It can also cause less severe infections, such as vaginal candidiasis, in healthy individuals under certain conditions that cause disturbance to normal flora, like taking antibiotics[1,2,4]. The mortality rate of *C. albicans* infections is reported to be up to 50%[5], and the ability of these fungal pathogens to develop resistance to current antifungal treatments is even increasing the death caused by *Candida* infections[6,7].

1.1.1 Candidiasis treatments

Different classes of antifungal agents have been used to treat infections caused by *C. albicans* and other *Candida* species including azoles, echinocandins and polyenes (Figure 1.2)[1,2,8].

Azoles are a large family of Food and Drug Administration (FDA)-approved antifungals which includes fluconazole, itraconazole, voriconazole, and posaconazole[2]. Azoles target the lanosterol 14-α-demethylase and inhibit its enzymatic activity for biosynthesis of the ergosterol, one of the important components of the yeast's cell membrane, thus disrupting the cell membrane[2]. Some *C. albicans* strains have shown

an intrinsic resistance (meaning they are naturally resistant) to one or more members of the azole family, and resistance can also develop over the course of treatment of *C. albicans* infection with azoles [1].

Another FDA-approved family that is prescribed to patients with invasive candidiasis is echinocandins, including anidulafungin, caspofungin, and micofungin. This family is a lipopeptide antifungal agent that disturbs the fungal cell wall by inhibiting the enzyme (1,3)-β-D-glucan synthase, which is responsible for production of glucan. In most cases, echinocandins are prescribed as an alternative to people with azole resistant candidiasis, but *Candida* can gain resistance to this family as well[2,9].

Polyenes are another frequently used antifungal family. This family includes amphotericin B and nystatin. This antifungal family, like the azoles and echinocandins, targets ergosterol and kills *Candida* by invading the cell membrane through an aqueous pore formation by binding ergosterol. The pore causes leakage of the components of the cytosol leading to cell death. Although *Candida* species have developed minimal resistance to amphotericin B over the years, the toxicity and side effects of polyenes limits their use[9].

Considering the limitations of currently available antifungal agents, such as adverse effects, drug-drug interactions, and gaining resistance, developing new technology to treat fungal infections is of high importance[9].

1.2 Cell-penetrating peptides (CPPs)

To help drive the development of new antifungal agents forward, we have studied the use of cell-penetrating peptides (CPPs) to deliver molecules into fungal cells. CPPs can cross the cell membrane and take other molecules with them, and they are a promising tool in drug delivery. Understanding their interaction with molecules that need assistance in crossing the cell membrane to reach intracellular targets is necessary.

1.2.1 The cell membrane as a barrier to intracellular delivery

In recent decades, much research has been done for the intracellular delivery of therapeutic agents, but the hydrophobic nature of the cellular membrane is a big barrier for bioactive molecules that are hydrophilic to enter the cells (Figure 1.3)[10]. The amphipathic phospholipid bilayer, with its hydrophilic portion facing the outside environment of the cells, selectively rejects the entrance of charged ions of any sizes and large polar molecules, including amino acids [11], so a strategy to deliver these molecules to the cytoplasm is required. Drugs have been delivered using several methods, including liposomes, polymeric micelles, and viral vectors, but there are problems with using these systems like low efficiency, toxicity towards cells, and low biocompatibility[12].

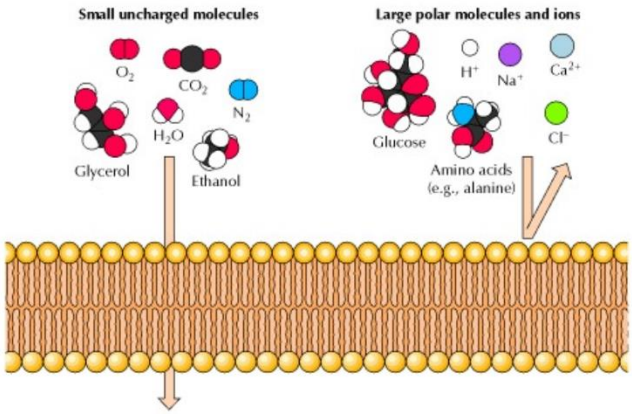

Figure 1.2 Selective permeability of cell membrane. Small uncharged polar or nonpolar molecules can cross, but the charged ions and charged or uncharged large polar molecules are rejected. Figure reproduced with permission of Geoffrey M Cooper through PLSclear. Copyright 2000 Oxford Publishing Limited [11].

1.2.2. CPPs as drug delivery agents

CPPs are short peptides, typically consisting of less than 30 amino acids, that can cross cell membranes and shuttle a wide variety of cargos inside the cells. So far, the translocation of CPPs by mammalian, plant, bacterial, yeast, and insect cells have been reported[13].

Up to now, no CPP or CPP-cargo complex has been approved by the FDA, although some drugs have been evaluated in the preclinical phase and the subsequent phases I, II and III trials [14]. One example of a CPP-facilitated therapy in the preclinical trial is the MPG-8-siRNA for cancer therapy. MPG-8 (AFLGWLGAWGTMGWSPKKKRK), is a shorter version of the peptide MPG that is engineered to make a stable complex with an siRNA and was tested in xenografted

tumor mouse models, successfully demonstrating reduction in the size of the tumor[14]. The first CPP-derived drug that entered a clinical trial was the conjugation of a polyarginine to cyclosporine A the CsA (PsorBan; CellGate, Inc.) to treat psoriasis. Cyclosporine A can be used for the treatment of psoriasis, but it is ineffective due to lack of mechanism for entrance into the dermis of human skin[15]. The CPP-based drug passed phase I of the clinical trial, but phase II was discontinued due to the slow rate of releasing the drug[14,15].

1.2.3. Translocation mechanisms

The exact mechanism of translocation of CPPs varies from one CPP to another and can depend on the experimental conditions. Endocytosis and direct translocation are mechanisms that are reported for CPPs (Figure 1.4)[12]. Endocytosis is an energy-dependent pathway, which the cell uses to selectively remove particles like food and nutrients, from the surface of the cell and take them inside. Endocytosis can be further divided into macropinocytosis, endocytosis mediated by caveolae or clathrin receptor proteins, and caveolae- and clathrin-independent endocytosis[12,16,17] (Figure 1.3). In macropinocytosis, dynamin proteins participate in the development of new vesicles from the cell membrane's exterior surface, called macropinosomes [16]. This pathway needs a stimulus to function, like growth factors or viruses[12]. In receptor-mediated endocytosis, including caveolae- or clathrin-mediated uptake, after interaction and binding of the particles to the receptors, clathrin and caveolin proteins facilitate the formation of clathrin- or caveolin-coated (also called caveosome) vesicles [16](Figure 1.3). Depending on the nature of the CPP and its cargo, one or more pathways of

endocytosis are possible to be used by the same CPP for internalization into cells[12]. A challenge with energy-dependent uptake is the endosomal escape after internalization. If the CPPs get trapped in the vesicle, they will undergo lysosomal degradation[12].

The direct translocation pathway is an energy-independent penetration of CPPs, and it usually takes place in the presence of amphipathic CPPs at high concentrations. Direct translocation can occur through different mechanisms, namely, the inverted micelle formation, pore formation, carpet-like model, and membrane-thinning model[16]. In all these mechanisms, the uptake is activated after the CPPs are attracted to the membrane via electrostatic interactions. In the inverted micelle model, in addition to the attraction between negatively charged components of the membrane and the positively charged portion of the CPPs, the interaction between the hydrophobic parts of the membrane and the CPPs help the translocation[16]. Pore formation is described by different models, one being the toroidal model. In the toroidal model both, the CPP and the lipid participate in pore formation in a way that lipids curve to let the CPP get close to the lipid head groups, and the pore will form[16]. In the membrane thinning and the carpet-like model, respectively, the thinning and the carpeting of the membrane befalls because of the electrostatic interactions between the cationic CPP and the membrane, thus enabling the translocation[16].

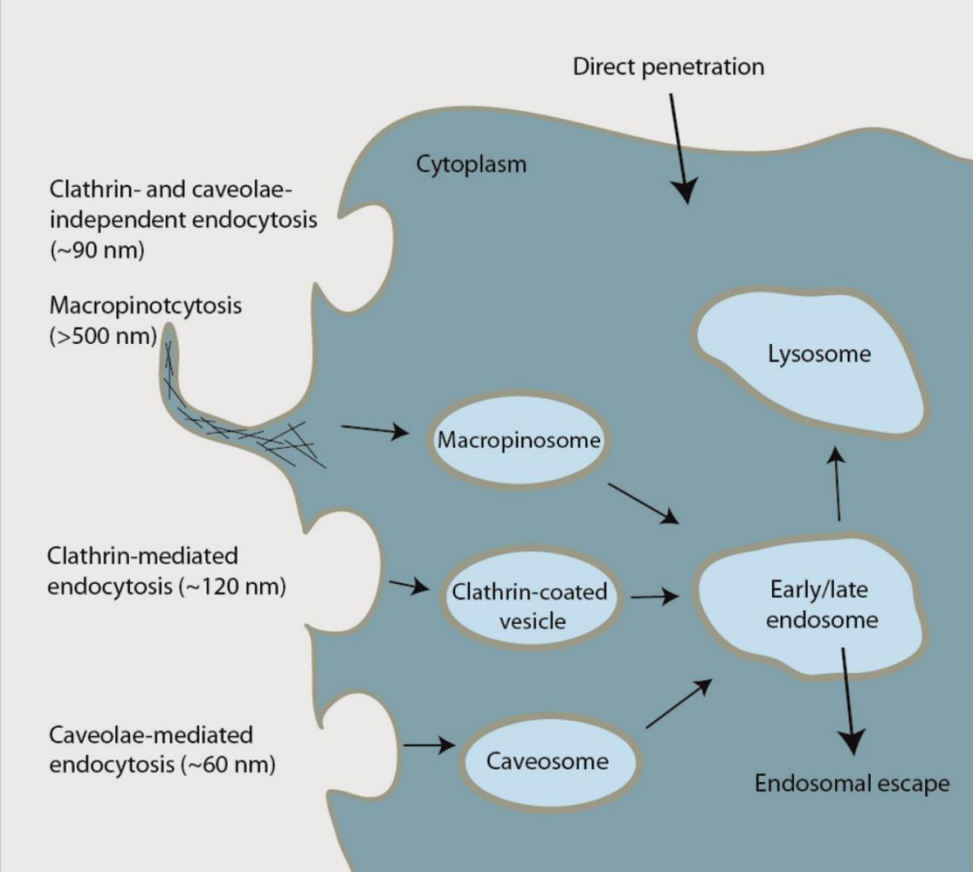

Figure 1.3 Different pathways for uptake and release of the cell-penetrating peptides. CPPs into the cells via different pathways. Figure reprinted with permission from Copolovici et al. Copyright 2014 American Chemical Society [12].

Many factors affect the mechanism of action of CPPs. For example, CPPs that take the endocytosis pathway at low concentration might employ direct translocation at higher concentration of peptide[16]. The secondary structure of the peptide also plays a role in the mechanism, since the secondary structure that CPPs adopt can affect the distribution of side chains with different properties. For example, a peptide upon formation of α-helix might become amphipathic[18]. Finally, the cell type is also important. types of cells

have different membrane composition, so the mechanism of action of each CPP should be studied for each type of cell separately[18].

1.2.4. Types of CPPs

CPPs are classified in many ways. One common way is to group them based on their physical-chemical properties: cationic, hydrophobic, and amphipathic CPPs (Table 1.1).

Cationic CPPs: Cationic CPPs are known for their high positive net charge and are mainly composed of the cationic amino acids namely, arginine, lysine, and histidine. Even if peptides are not cationic overall, many of them include positively charged residues in their structures[12], since the positive charges are important to initiate binding to the negatively charged phospholipid bilayer of the membrane[13]. Based on the data for a number of cationic CPPs, at least eight positively charged residues are required for the efficient uptake by the cells[19,20]. Examples of cationic peptides include polyarginines and penetratin[10] (Table 1.1). The nuclear localization sequences (NLS) that target peptides to the nucleus are members of the cationic CPP classification[10]. It is worth mentioning that some cationic CPPs can impact cell viability and membrane integrity[19].

Hydrophobic CPPs: Hydrophobic CPPs are made up primarily of residues with polar side chains[12]. They have low net charge, but their hydrophobicity is an important factor in their translocation into the cell. Only a few hydrophobic CPPs have been discovered

to-date (for example, C105Y and Pep-7; Table 1.1), and it has been suggested that these CPPs can translocate into the cells via an energy-independent mechanism[14].

Amphipathic CPPs: Amphipathic CPPs have both a charged domain and a hydrophobic domain. They are divided into two subgroups of primary and secondary amphipathic CPPs[14]. Primary amphipathic CPPs have charged and hydrophobic domains on opposite ends of the primary sequence of the peptide. They can be chimeric constructs obtained from the combination of a cationic CPP with a hydrophobic domain, such as the peptide MPG and Pep-1 (Table 1.1), or can be naturally derived from proteins, such as pVEC[14,16] (Table 1.1). Secondary amphipathic CPPs are those that, after the transition to a secondary structure like an α-helical structure, form an amphipathic structure by having hydrophilic residues on one side and hydrophobic residues on the other side, like MAP[14].

Table 1.1 CPP sequence, origin and classification based on cationic, hydrophobic, and amphipathic. Table recreated from[12,14]

CPPs	Sequence	Origin
	Cationic	
Penetration	RQIKIWFQNRRMKWKK	Antennapedia homeodomain
Polyarginines	R_n	Synthetic
	Amphipathic	
MPG	GALFLGFLGAAGSTMGAWSQPKKKRK	HIV glycoprotein 41/SV40 T antigen NLS
pVEC	LLIILRRRIRKQAHAHSK	Vascular endothelial cadherin
MAP	KLALKLALKALKAALKLA	Chemically synthesized

Pep-1	KETWWETWWTEWSQPKKKRKV	Tryptophan-rich antigen NLS	cluster/SV40T
	Hydrophobic		
C105Y	CSIPPEVKFNKPFVYLI	a1-Antitrypsin	
Pep-7	SDLWEMMMVSLACQY	CHL8 peptide phage clone	

1.2.5. CPP-cargo attachment

Regardless of the limited knowledge of how CPPs exactly pass through the membrane, their ability to do so is exploited to deliver therapeutics into the cells[10]. The attachment of cargo to CPPs can occur through covalent bonding or non-covalent interactions (Figure 1.4). In covalent bonding, the cargo and CPP are linked together through a covalent bond. In this case the position of cargo with respect to the CPP needs to be considered. The cargo can be attached to the N- or C-terminus of the CPP or to the side chain of an amino acid within the peptide. Examples of covalent bonds used to attach cargo to CPPs are disulfide bonds and peptide bonds[20,21]. Genetic fusion of a protein cargo to a CPP and recombinantly expressing the fusion CPP-cargo takes advantage of the covalent attachment through a peptide bond. Using covalent linkage of cargo to the peptide has the advantage of controlled release of cargo inside the cells, like how a disulfide bond is reduced in the reducing environment of the cells thus releasing the drug[20]. Another reason that covalent linkage sometimes is preferred over noncovalent linkage is that it facilitates the production of larger and more complex protein cargos attached to CPP [20–22].

Non-covalent attachment of cargo to the CPP involves interactions of the CPP with the surface of the cargo through electrostatics, π-π stacking, hydrophobic interactions, or H-H bonds[23]. The complex formed by non-covalent bonds can be very challenging to characterize, since formation of aggregates leads to complicated secondary and tertiary structures[12]. One common example of non-covalent bonding is the attachment of negatively charged DNA backbone to the cationic CPPs via electrostatic interactions[20].

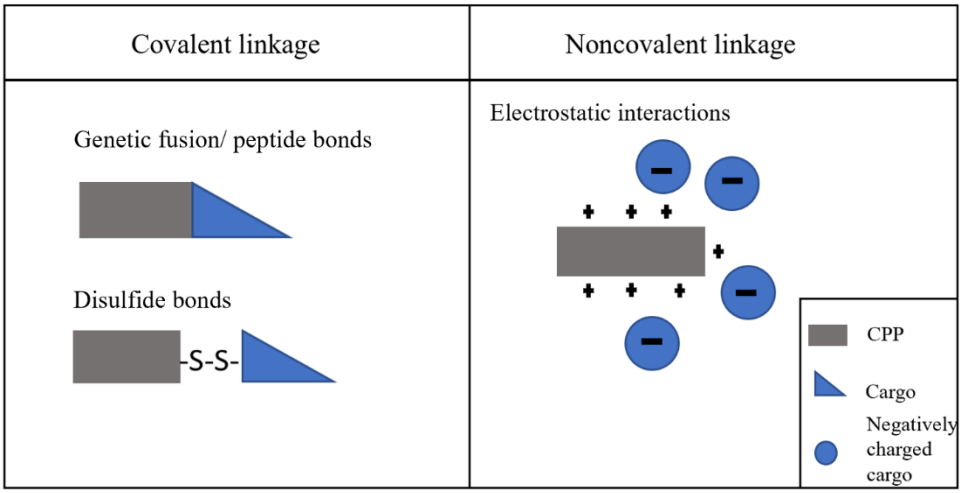

Figure 1.4 Examples of different methods of cargo attachment to the CPP. Cargo is attached to CPPs via covalent bond or non-covalent. Figure is recreated from [20].

1.3CPPs and C. albicans *cells*

Since the introduction of CPPs and their unique ability to carry a large variety of cargos across the cell plasma membrane, researchers have contributed to over 2000 papers about CPPs[15]. Most of the studies done on CPPs have focused on their application in mammalian cell lines, and little work has been done to study their translocation into fungal cells[18,24–26]. In this part of the thesis, some of the work that has been done on understanding the interaction of CPPs with fungal cells is reviewed.

1.3.1 Mechanism of entry into C. albicans

Although many of CPPs have been characterized for their mechanism of entry into mammalian cells, this mechanism may be different in fungal cells due to the presence of the cell wall and different cell-surface proteins in fungal cells[25]. Gong et al. investigated the mechanism of entry of some peptides into the *C. albicans* and compared the results to published mechanisms in mammalian cells[25] (Table 2). They found the mechanism of translocation of the CPPs is variable, and it highly depends on the CPP being used and the type of cell in the experiment[25].

Table 1.2 Comparison of translocation mechanism in fungal cells and mammalian cells.

Recreated from [25].

Peptide	Sequence	MW (Da)	Mechanism in mammalian cells*	Mechanism in fungal cell*
pVEC	LLIILRRRIRKQAHAHSK	2209.7	M	E/M
MAP	KLALKLALKALKAALKLA	1876.0	E	E/D
synB	RGGRLSYSRRRFSTSTGR	2100.3	E	E
MPG	GALFLGFLGAAGSTMGAWSQPKKKRKV	2807.4	D	E
hCT	LGTYTQDFNKTFPQTAIGVGAP	2323.6	E	ND
Penetratin	RQIKIWFQNRRMKWKK	2246.8	M	M/D

*The mechanisms are listed as endocytosis (E), direct translocation (D), micropinocytosis (M), or no translocation detected (ND).

The secondary structure that the CPPs adopt in the aqueous environment may differ from the structure gained in the presence of different cell types. Many factors like the overall charge, hydrogen bonds, environment, and helical properties of the peptide might cause changes in the secondary structure of the CPPs[12]. Thus, understanding the secondary structure of the peptides is important in studying the CPP-membrane

interaction and translocation[12]. Circular dichroism (CD) was used by Gong et al. to study the secondary structure of the CPPs in different environments and in the presence of live cells. Subsequently, the results were combined with Monte Carlo simulations with a model membrane to better understand the CPP-membrane interaction and the translocation mechanism[18]. The Monte Carlo simulations showed the main driving force for the interaction of the CPPs with the cell membrane was the electrostatic interactions between the positively charged residues and the lipid bilayer. For peptides expected to translocate via a direct translocation mechanism (Table 1.2), the simulations showed the peptides interacted with the hydrophobic portion of the membrane, and these peptides, which require a hydrophobic environment to form their α-helical secondary structure, also exhibited α-helical structure in the CD with live cells. For peptides expected to translocate by endocytosis, the Monte Carlo simulation predicted no secondary structure formation, and the driving force for internalization was still the electrostatic interactions. These results indicate that these peptides attached to the cell membrane but did not interact with the hydrophobic portion of the membrane, and they translocated via an energy dependent pathway.

1.3.2 Translocation of CPP into C. albicans *cells*

The translocation of different model cargos into *C. albicans* cells has been studied previously. Some CPPs efficiently caried a fluorescein fluorescent label as their small-molecule model cargo into the *C. albicans* cells[25]. Among the peptides that were studied for translocation into the cells, pVEC, MAP, synB, penetratin, and MPG showed the best translocation results, but the toxicity of MAP, pVEC and penetratin

towards the cells was high, indicating these peptides can act as an antifungal peptide while translocating.

The ability of CPPs to carry a large cargo fused to its N- or C-terminus inside the cells has also been evaluated[27]. The model cargo was typically green fluorescent protein (GFP) which is 27 kDa in size. A number of peptides have been reported to carry GFP into *C. albicans* cells with the GFP attached to the C-terminus of the peptide, including pVEC, MAP and MPG, though the level of translocation varied[25]. Of particular interest to this thesis, previous work in our lab showed that MPG attached to GFP carried the cargo into about 40% of *C. albicans* cells[27]. In this case, the GFP was attached to the N-terminus of the peptide, with no work to understand if this was the best orientation of the CPP and cargo.

1.4 Overview of the thesis

In this thesis, we studied the best location of the protein cargo, with respect to the peptide MPG, to efficiently translocate the cargo into *C. albicans* cells. We studied the translocation of constructs with GFP fused to the N- and C-terminus of MPG. In Chapter 2, detailed experimental processes are described for the construction, expression, extraction, and purification of the constructs, as well as the process for quantification of their translocation into the *C. albicans* cells. The analysis of the results of the experiments and discussions of the data are presented in Chapter 3. Finally, in Chapter 4, we present our conclusion of the work and propose ideas for designing new experiments to improve the validity of our results.

Chapter 2: Material and methods

2.1 Recombinant protein design and construction

Two different fusion proteins with the cargo at the N-terminus of the fusion protein were built for this study: one with the T7 tag at the N-terminus and the other without the T7 tag. The fusion protein with the cargo at the C-terminus of the CPP was constructed for a previous study29–31.

2.1.1 Cloning

The CPP fusions to GFP and controls with no CPP were cloned into the pET21(a)+ plasmid (Novagen) for expression. The plasmids created and the primers used in this study are listed in Tables 4 and 3, respectively. The primers were all designed for this study and commercially synthesized (IDT DNA or Genewiz).

Table 2.1 Oligonucleotide sequences

Oligonucleotide sequence name	**Sequence (5' to 3')**
GFP-FWD1	TTGTTTAACTTTAAGAAGGAGATATACATATGCACCACCACCAC CACCACATTGAGGGAC
GFP- FWD2	TAGCTGAATTCACATGCACCACCACCACCACCACATTGAG
GFP-REV1	CACGAGTCGACTTTGTATAGTTCATCCATG
GFP-Stop-Rev	GCAGTCGACTCATTTGTATAGTTCATCCATGC

6XHis-GFP-FWD1	CATCATCACCACCACCACAGTAAAGGAGAAGAACTTTTC
ECORI-FacXa-FWD2	ATTCAAGAATTCATCGAAGGTCGTCATCATCACCACCAC
MPG Top1	TCGACGGAGGCGGTGGAAGCAAGCTTGGCGCACTTTTCTTAGG GTTCCTTGGAG
MPG-Bottom1	GCGGCTCCAAGGAACCCTAAGAAAAGTGCGCCAAGCTTGCTTC CACCGCCTCCG
MPG-Top2	CCGCCGGGAGTACGATGGGTGCCTGGTCCCAGCCAAAGAAGAA ACGTAAAGTATAGGC
MPG-Bottom2	GGCCGCCTATACTTTACGTTTCTTCTTTGGCTGGGACCAGGCAC CCATCGTACTCCCG
HindIII-pVEv-Top1	AGCTTTTGTTAATTATACTACGTAGACGAATA
HindIII-pVEC-Bottom1	TTCCTTATTCGTCTACGTAGTATAATTAACAAA
pVEC-NotI-Top2	AGGAAGCAGGCGCATGCTCACAGCAAATGAGC
pVEC-NotI-Bottom2	GGCCGCTCATTTGCTGTGAGCATGCGCCTGC
HindIII-MAP-Top1	AGCTTAAACTTGCTTTGAAATTAGCCTTAAA
HindIII-MAP-Bottom1	CGCCTTTAAGGCTAATTTCAAAGCAAGTTTA
MAP-NotI-Top2	GGCGCTGAAGGCGGCATTAAAGCTGGCTTGAGC

MAP-NotI-Bottom2	GGCCGCTCAAGCCAGCTTTAATGCCGCCTTCAG

Table 2.2 List of plasmids. All the constructs are inserted into pET21a(+) plasmid

Plasmid name	Relevant characteristics	Reference
MPG-G_4S-GFP	GFP fused to the C-terminus of MPG, C-terminal 6×His, G_4S linker between GPF and MPG	29,32
GFP-G_4S-MPG	GFP fused to the N-terminus of MPG, N-terminal 6×His tag, factor Xa site after 6×His, G_4S linker between GPF and MPG	This study
GFP-6×His	C-terminal 6×His tag	This study
T7-6×His-GFP	N- terminal T7 tag followed by a factor Xa site and 6×His tag.	This study
T7-GFP-G_4S-MPG	GFP fused to the N-terminus of MPG, N-terminal T7 tag followed by a factor Xa site and 6×His tag, G_4S linker between GPF and MPG	This study

To construct the plasmids GFP-G_4S-MPG and 6×His-GFP, we first amplified GFP from the MPG-G_4S-GFP plasmid listed in Table 2.229,32, using a two-step polymerase chain reaction (PCR) amplification. Primers GFP-FWD1 and GFP-REV1 were used for the first step. For the GFP-G_4S-MPG plasmid, the PCR product of first step was directly used as a template for the second step of PCR amplification using GFP-FWD2 and GFP-REV1 primers. For the 6×His-GFP plasmid, which served as a negative control to make sure GFP will not translocation into the cells by itself, the same product from the first PCR step of GFP amplification was used as the template for the second step of PCR amplification with primers GFP-FWD2 and GFP-Stop-Rev to add a stop codon and terminate the transcription of any gene after GFP ends. The final second-

step PCR products were purified (Wizard CV kit, Promega) and digested with EcoRI (New England Biolabs) and SalI-HF (New England Biolabs) restriction enzymes to prepare for insertion into the plasmid.

The DNA encoding MPG and the linker was prepared via dimerization of two pairs of complementary DNA oligonucleotides (Figure 2.1) (Pair 1: MPG-Bottom1 and MPG-Top1; Pair 2: MPG-Bottom2 and MPG Top2). The DNA coding for the G_4S peptide linker and the CPP with sticky ends complementary to SalI and NotI restriction sites was included in the oligonucleotide design for easy insertion into the plasmid. The BamHI restriction site was included between the linker peptide sequence and the CPP to facilitate exchange of the CPP DNA in the plasmid to encode other CPPs. To prepare the oligonucleotide dimers for insertion into the plasmid, the 5' ends of the complementary oligonucleotides were phosphorylated using T4 polynucleotide kinase (New England Biolabs) and annealed together in a C1000 thermal cycler (Bio-Rad) programmed to incubate at 95 ℃ for 2 min and cool down to 20 ℃ over 15 min to form a double-stranded DNA construct. The oligonucleotides MPG-Bottom1 and MPG-top1 were annealed together and formed a double-stranded DNA construct with a 5' sticky end for the SalI restriction enzyme site and with a 3' end containing a complementary overhang to the 5' end of the annealed MPG-Top2 and MPG-Bottom2 DNA construct, which had a 3' sticky end for the NotI restriction enzyme site.

The pET21a(+) plasmid was digested using EcoRI and NotI-HF enzymes to prepare for insertion of the GFP and MPG DNA. The designed plasmid and the double-stranded

DNA encoding for GFP, and MPG were ligated together using T4 DNA ligase (New England Biolabs) at 16 ℃ overnight, producing the GFP-G_4S-MPG and 6×His-GFP plasmids (Figure 2.1).

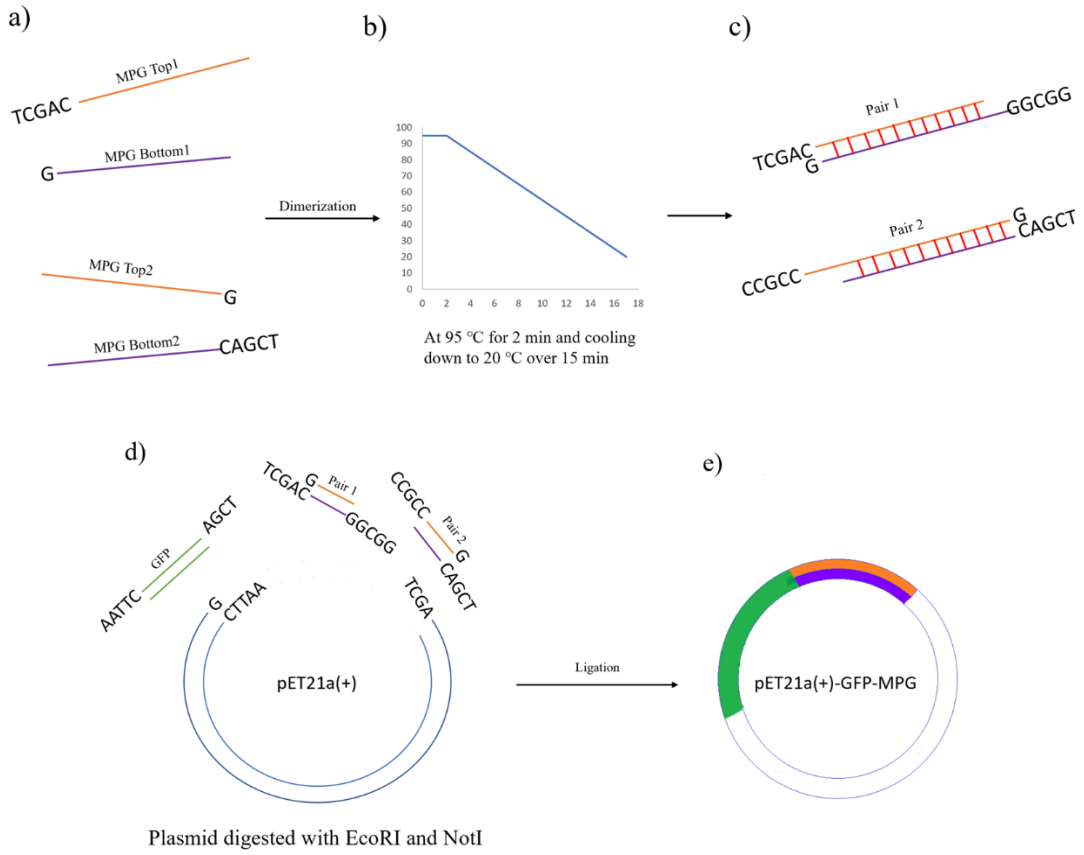

Figure 2.1 Schematic overview of the oligonucleotide dimerization and insertion into pET21a (+) vector. (a) Pairs of complementary oligonucleotides were designed, (b) dimerization was done in a thermal cycler, (c) the hydrogen bonding between G-C and A-T base pairs created: Pair 1 with sticky end for SalI restriction enzyme site and Pair 2 with sticky ends for NotI restriction enzyme site, (d) pET21a (+) was digested with NotI and EcoRI, and (e) MPG and GFP DNAs were ligated into the vector. The sticky ends are shown by appropriate complementary base pairs.

For the plasmids containing the T7 tag with MPG and without MPG, a similar process was used, except the primers were different. GFP was amplified from the MPG-G_4S-GFP[1,4] using primers 6×His-GFP-FWD1 and GFP-REV1. To construct the T7-GFP-G_4S-MPG plasmid, the amplified GFP was used as a template for another PCR step using primers ECORI-FacXa-FWD2 and GFP-REV1, while for the T7-6×His-GFP plasmid, the primers ECORI-FacXa-FWD2 and GFP-Stop-Rev were used. The resulting plasmids were T7-GFP-G_4S-MPG (Figure 2.2a).

a)

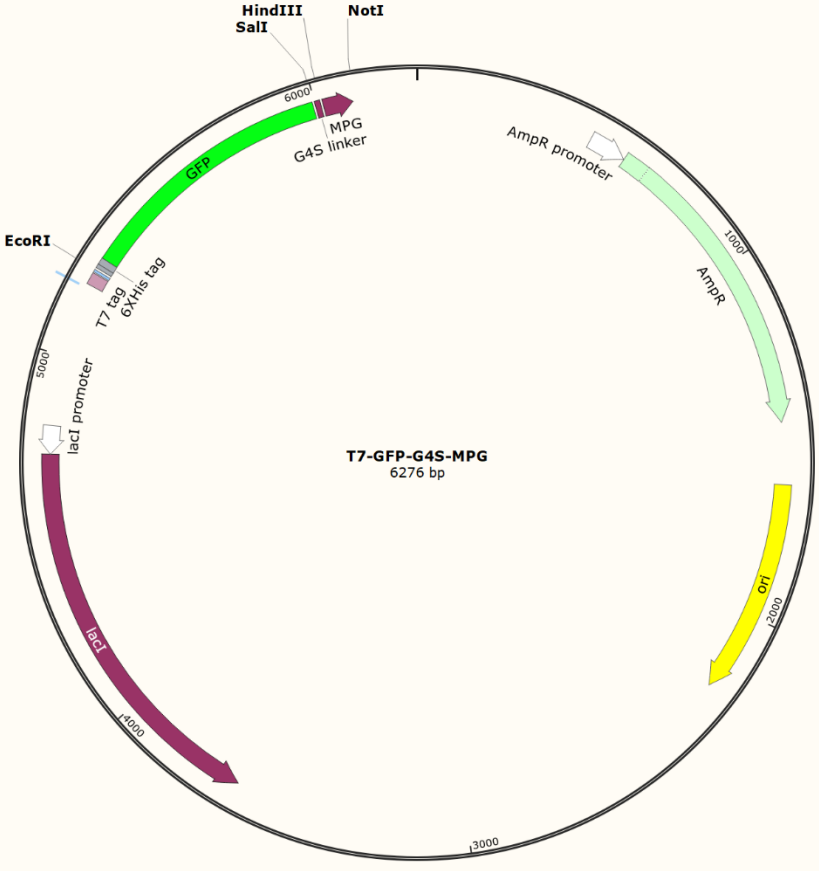

b)

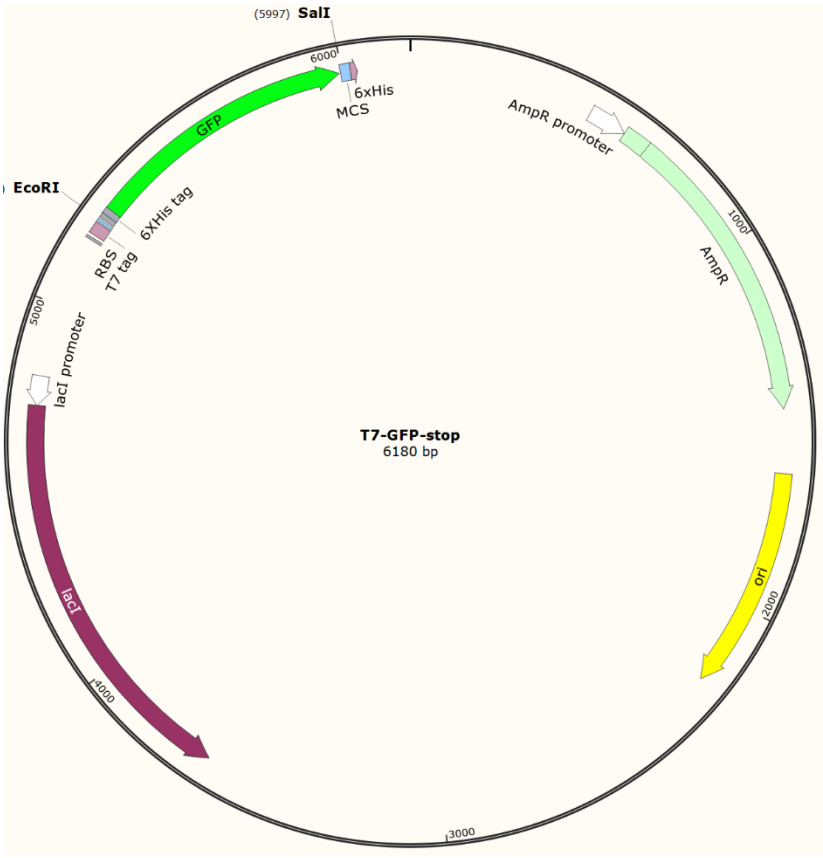

Figure 2.2 Plasmid maps. a) Plasmid map of T7-GFP-G_4S-MPG and b) T7-GFP-6×His. The relevant restriction enzyme sites are shown on the figure.

2.1.2 Transformation and screening

The circular DNA obtained from the ligation step was transformed into electrocompetent cells of the *E. coli* BL21(DE3) strain (Novagan) via electroporation. BL21(DE3) contains the gene for the expression of T7 RNA polymerase under regulation of the lacUV5 promoter, which is inducible by isopropyl β-D-1-thiogalactopyranoside (IPTG)33,34. BL21(DE3) was used as the host strain for expression of the target gene. The ligation product was desalted and added to a

BL21(DE3) electrocompetent cell suspension, and then the cell suspension was shocked using Gene Pulser Xcell instrument (Bio-Rad). The cells were allowed to recover for 1 h in super optimal broth with catabolite (SOC) media (2% tryptone, 0.5% yeast extract, 10 mM NaCl, 2.5 mM KCl, 10 mM $MgCl_2$, 10 mM $MgSO_4$, and 20 mM glucose) at 37 ℃ while shaking at 225 RPM before spreading the cells on LB agar plates (15 mg/mL agar, 10 mg/mL tryptone, 10 mg/mL NaCl and 5 mg/mL yeast extract) containing ampicillin 100 μg/mL and IPTG at 0.01 mM.

After overnight incubation of the plate at 37 ℃, we picked 3 or 4 colonies that were green (indicating GFP expression) from the plate and grew them overnight in Luria Bertani (LB) liquid medium (10 mg/mL tryptone, 10 mg/mL NaCl and 5 mg/mL yeast extract) containing ampicillin (100 μg/mL). DNA was extracted from the culture for each colony using the Wizard Promoga miniprep kit according to the manufacturer's protocol. The purified DNA was further screened for insertion of CPPs via PCR amplification using appropriate primers. For example, for 6xHis-GFP-G_4S-MPG, we used MPG-Top1 and MPG-Bottom2 for the PCR screening. The size of the PCR product was visualized in a 1% agarose gel to confirm a band around 100 base pairs depending on the size of the DNA encoding for the CPP. After screening for GFP expression and CPP gene presence, we sent the plasmids that passed both tests for Sangar sequencing (Genewiz) to confirm the sequences. A freezer stock was prepared from each overnight culture for long-term storage by mixing a 1:1 volume ratio of 50% glycerol and the overnight culture.

2.2 Protein expression

To express protein for downstream assays, we grew the cells overnight from the freezer stock in 20 mL liquid LB media containing ampicillin (100 μg/mL). After overnight growth at 37 °C while shaking at 225 RPM, the optical density at 600 nm was measured, and cells were subcultured into 1000 mL of fresh LB media containing ampicillin to an optical density at 600 nm of 0.05. After growing the subculture for about two and half hours at 37 °C while shaking at 225 RPM, production of the target protein was induced by adding IPTG (Fisher Bioreagents) to a final concentration of 0.01 mM. Six hours after beginning induction, cells were harvested via centrifugation at 4300 × g and 4 °C for 20 min. We discarded the supernatant and saved the pellet for extraction and purification of desired protein.

2.3 Target protein extraction and purification

2.3.1 Protein extraction

Cell pellets were resuspended in 17 mL of equilibration buffer (500mM NaCl, 50mM sodium phosphate (NaPB), pH 7.5). A 25 μL volume of 100× protease inhibitor stock (MilliporoSigma) was added to the suspension to inhibit the protease activity. In cases where the suspension was viscous, 10 μL of benzonase nuclease (MilliporeSigma) was added to the suspension. The cell suspensions were then lysed using a homogenizer cell disruption system (Avestin, Inc.) and centrifuged to separate the cell debris from the solution containing soluble proteins. After centrifugation at 11400 × g for 45 mins,

supernatant (hereinafter known as “lysate”) was saved and passed through a 0.45 μm sterile filter and saved for downstream assays.

2.3.2 Protein purification

The protein purification was done using immobilized metal affinity chromatography (IMAC). The nickel-charged iminodiacetic acid (NIDA) resins for IMAC and appropriate columns were purchased from Bio-Rad, and about 5 mL of resin was loaded to each column. After equilibrating the column with 5 column volumes of equilibration buffer (500mM NaCl, 50mM NaPB, pH 7.5), the lysate was loaded onto the column, and the column was incubated with rotation for 45 mins at room temperature or up to 2 h at 4 ℃. After incubation, the flowthrough of each column was collected, and the resin was washed with 5 column volumes of equilibration buffer to remove residual unbound proteins. This wash was collected as Wash 1. The column was then washed with equilibration buffer containing 10 mM imidazole to remove any loosely bound proteins, and this wash was collected as Wash 2. Finally, the target protein was eluted using buffer containing 300 mM imidazole (500mM NaCl, 50mM NaPB, 300 mM imidazole, pH 7.5).

2.4 Sodium dodecyl sulfate polyacrylamide gel electrophoresis (SDS-PAGE)

After purification, we analyzed the collected flowthrough, Wash1, Wash2 and eluate on an SDS-PAGE gel. The concentration of samples was estimated with the Beer-

Lambert Law, using a Nanodrop instrument (Thermo Scientific) to measure the absorbance at 280 nm and the extinction factor and size for each sample noted in Table 2.3. A 20 µL solution containing 2 µg of protein and 1× SDS-dye (0.05 M Tris-HCl, 0.1 M dithiothreitol (DTT), 8% (w/v) SDS, 1.5 mM bromophenol blue, and 1.075 M Glycerol) was prepared and heated at 98 ℃ for 5 min to denature the protein. Then 15 µL of solution was loaded to an Any KD Mini-Protein TGX 15-well gel (Bio-Rad) along with a molecular weight marker (Precision Plus Protein Standards; Bio-Rad). The gel was run at 200 V for 30 mins to separate fragments based on their size. The gel was stained using Bio-Safe Coomassie (Bio-Rad) according to the manufacturer's protocol and imaged using a ChemiDoc MP documentation system (Bio-Rad). The purity of the target protein in the eluate was determined using densitometry.

Table 2.3 Molecular weight, PI, and extinction factor for the constructs

Sample	**M_W (kDa)**	**Extinction factor ($cm^{-1}M^{-1}$) ***
T7-GFP-G_4S-MPG	33	22515
MPG-G_4S-MPG	30	22515
T7-6×His-GFP	29.67	22015
T7-GFP-6×His	30.045	22015
GFP-6×His	28.14	22015

*Extinction factors were calculated using Expasy's ProtParam tool at https://web.expasy.org/protparam/.

2.5 Western blot

To compare the expression level of different constructs, we performed Western blotting. A 5 ml overnight culture in LB broth liquid media (10 mg/ml tryptone, 10 mg/ml NaCl, and 5 mg/ml yeast extract) containing ampicillin was prepared and subcultured into 10 mL fresh LB media as described for protein expression (Section 2.2). After 2.5 h of shaking at 225 RPM and 37 ℃, IPTG (Fisher BioReagents) was added to a final concentration of 0.01 mM, and 6 h after the beginning of induction, the cells were harvested at 4300 × g and 4 ℃ for 20 mins. The cell pellet was lysed using BugBuster Master Mix (EMD Millipore) according to the manufacturer's protocol to extract proteins in the soluble fraction of the cells. In cases where proteins were not detected in the soluble fraction, protein in inclusion bodies was recovered according to the BugBuster manufacturer's protocol. The absorbance at 280 nm of the solution containing proteins (soluble or insoluble) was measured using a Nanodrop 2000 Spectrophotometer instrument to estimate the total concentration of proteins in the sample. The same mass of total protein for each sample was loaded onto a gel for separation by SDS-PAGE (Section 2.4). After separation by SDS-PAGE, the proteins were transferred to a polyvinyl difluoride (PVDF) membrane using the Trans-Blot Turbo instrument (Bio-Rad). Then the membrane was blocked by incubation in 5% (w/v) non-fat dry milk in Tris-buffered saline containing Tween-20 (TBST; 0.1% Tween-20, 50 mM Tris-HCl pH 7.5, 150 mM NaCl) for an hour at room temperature or overnight at 4 ℃. After blocking, the membrane was washed three times with TBST. We incubated the membrane with appropriate dilutions of the horseradish peroxidase (HRP)-conjugated anti-6×His tag antibody (Abcam) and/or HRP-conjugated anti-GFP antibody (Abcam) according to the manufacturer recommended concentrations for an

hour at room temperature. After the incubation with antibodies, the membrane was washed 6 times with TBST buffer. Clarity Western ECL substrate (Bio-Rad) was added to the membrane, and the membrane was incubated for 5 mins. The chemiluminescence was imaged on a ChemiDoc MP documentation system to visualize the protein on the blot.

2.6 Size exclusion chromatography (SEC)

To see if the purified protein sample contained soluble aggregates, we performed SEC. An Enrich-650 high resolution SEC column (Bio-Rad) was attached to the NGC liquid chromatography instrument (Bio-Rad). Phosphate-buffered saline (PBS; 137 mM NaCl, 2.7 mM KCL, 10 mM Na_2HPO_4, 1.8 mM KH_2PO_4, pH 7.5) was used as the mobile phase, and the column was equilibrated with two column volumes (the volume of Enrich 650 is 25 mL) of PBS. Before applying the sample, the column was calibrated using the gel filtration standard (Bio-Rad) (Table 2.4). The purified proteins were adjusted to the desired concentration and passed through a 0.2 μm filter before applying to the column. A volume of 100 μL of samples concentrated to 200 μM were applied to the column, and the system was at a flow rate of 1 mL/min in PBS. The absorbance at 280 nm was measured at the column exit. ChromLab software (Bio-Rad) was used to visualize the data.

Table 2.4 SEC standard proteins and their approximate elution volume.

Protein	Size (kDa)	Elution volume (mL)

Thyroglobulin	670	~10
Bovine γ-globulin	158	~12
Chicken ovalbumin	44	~14
Equine myoglobin	17	~15.5
Vitamin B12	1.35	~18

2.7 Quantification of translocation of GFP into C. albicans *cells*

We quantified and compared the translocation of GFP fusions to MPG into *C. albicans* cells using flow cytometry.

2.7.1 C. albicans *cell growth and preparation*

The *C. albicans* SC5314 strain (American Type Culture Collection) was streaked on a yeast-peptone-dextrose (YPD) agar plate (1% yeast extract, 2% peptone, 2% glucose, and 2% agar) and incubated at 30 ℃ for 24 h. We picked a random colony, inoculated it into 5 ml of YPD liquid medium (1% yeast extract, 2% peptone, and 2% glucose), and grew the culture overnight at 30 ℃ while shaking at 230 RPM. The overnight culture was subcultured into 5 ml of fresh YPD liquid medium to an optical density at 600 nm of 0.1 and incubated at 30 ℃ while shaking at 230 RPM. When the optical density at 600 nm reached 0.5, cells were pelleted by centrifugation at 3900 × g and washed 2 times with 10 mM NaPB (pH 7.5). Then cells were resuspended in 10 mM NaPB (pH 7.5) and diluted to an optical density at 600 nm of 0.3 (approximately 0.4×10^6 cells35).

2.7.2 Protein preparation for incubation with C. albicans *cells*

Each purified protein construct used in the flow cytometry assay was dialyzed against 10 mM NaPB (pH 7.5) using 10,000 molecular weight cut-off (MWCO) SnakeSkin dialysis tubing (Thermo Scientific) overnight at 4 ℃. The protein solutions were then concentrated to the desired concentration for the experiment using 10 kDa sample concentrators (Cytiva Vivaspin), according to the manufacturer's protocol.

2.7.3 Sample incubation and analysis with flow cytometry

Protein samples (100 μL) at 200 μM or 800 μM, depending on the experiment conditions, were added to 100 μL of the cell suspension prepared in Section 2.5.1. The samples were incubated at 30 ℃ for 1, 8, and 24 h to allow translocation of the protein fusions into the cells. After each incubation time was over, the cells were pelleted by centrifugation at 5,000 × g for 10 mins at 4 ℃. The supernatant was discarded, and the pellet was washed with 200 μL of 10 mM NaPB (pH 7.5) buffer. To remove any protein bound to the surface of cells, we incubated the cells with 200 μL of trypsin (Invitrogen) at 37 ℃ for 30 mins, as has been done previously in our lab30,32. After 30 mins, cells were pelleted at 5,000 × g for 10 mins at 4 ℃ and washed once with 200 μL of 10 mM NaPB (pH 7.5). Cells were resuspended in 200 μL of 10 mM NaPB (pH 7.5) and transferred to polystyrene flow cytometry tubes (Corning) to analyze samples for translocation of GFP using flow cytometry (BD FACSCantoII). To determine the membrane integrity after CPP translocation, propidium iodide (PI; PromoCell) was

added to a final concentration of 0.1 mg/ml in the samples right before analyzing with flow cytometry. Each cell was individually passed through a 488 nm excitation laser and 530/30 emission filter, and the emitted light was used to determine the percentage of PI- and FITC-positive cells for each sample. The experiment was done on 6 different days, and, for each day, a different batch of purified protein was used. On each day, two technical replicates were included.

2.7.4 Statistical analysis

Statistical analysis was done using GraphPad Prism 9.1.2. Since we had two independent variables in our analysis (time and proteins), we used a two-way ANOVA method, and Tukey's multiple comparison was performed to compare all the samples with one another. The threshold was set to $\alpha = 0.05$, and the P values were analyzed to determine the level of significance in the difference between the samples. A P-value smaller than α was significant.

Chapter 3: Results and discussion

3.1 Selection of the CPP and protein cargo

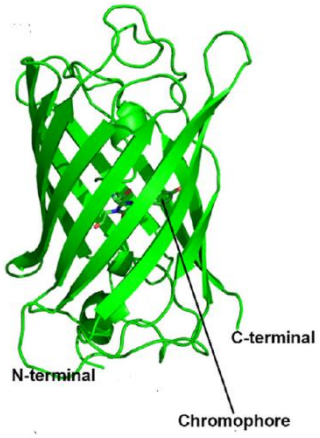

Figure 3.1 Crystal structure of GFP. The c- and N- terminal ends as well as the central chromophore are marked in the picture36**.** Figure reprinted with permission from Kong et al. Copyright 2020 Elsevier**.**

To study the ability of the CPPs to take molecular cargo into *C. albicans* cells, we selected GFP to serve as our model cargo. GFP, with its innate ability to emit green fluorescence, is a perfect candidate for tracking internalization of the construct using fluorescent microscopy or flow cytometry. GFP is originated from bioluminescent jelly fish *Aequorea victoria*[34,35]. It contains a p-hydroxybenzylidene-2-3-dimethylimidazolinone chromophore core, which is responsible for the green fluorescence (Figure 3.1). This motif is well protected from the outside environment by eleven β-sheets and two α-helices[35]. Wild-type GFP absorbs blue light at 395 nm and emits it at 510 nm[34]. GFP has widely been used in biological research due to ease of expression, detection, and high stability.

We selected MPG as our CPP delivery vehicle (Table 2). It is an amphipathic peptide consisting of 27 amino acids with a net charge of +3 not including charge from N-terminal free amine12,23,29. This peptide is a chimeric peptide which has two main domains: an N-terminal hydrophobic domain obtained from the fusion sequence of the HIV gp41 glycoprotein, and an NLS domain consisting of 6 residues (KKKRKV) derived from the SV40 large T-antigen12,38. These two domains are linked together with a sequence of 4 amino acids, which provides flexibility and stability for both

motifs due to the presence of proline12,32. MPG has been previously studied in our lab, and its mechanism of action and translocation into *C. albicans* cell is characterized20,23,27,29. With that in mind, we found it a good CPP for our study to determine the best position for the attachment of the cargo.

3.2 Cloning and design of the construct

The main purpose of this study was to find the preferred position of cargo with respect to the CPP for the highest translocation level into *C. albicans* cells. We designed a construct where GFP is fused to the N-terminus of a CPP (GFP-G_4S-CPP) (Figure 2.1a,b) and compared its translocation to the construct where GFP is fused to the C-terminus of CPP (CPP-G_4S-GFP) (Figure 2.1c), which was made and tested for translocation previously in our lab[2]. Negative controls for the GFP-G_4S-CPP fusion that lacked the CPP were also made (Figure 2.1a, b), and the previously designed negative control for the CPP-G_4S-GFP fusion (Figure 2.1c) was used.

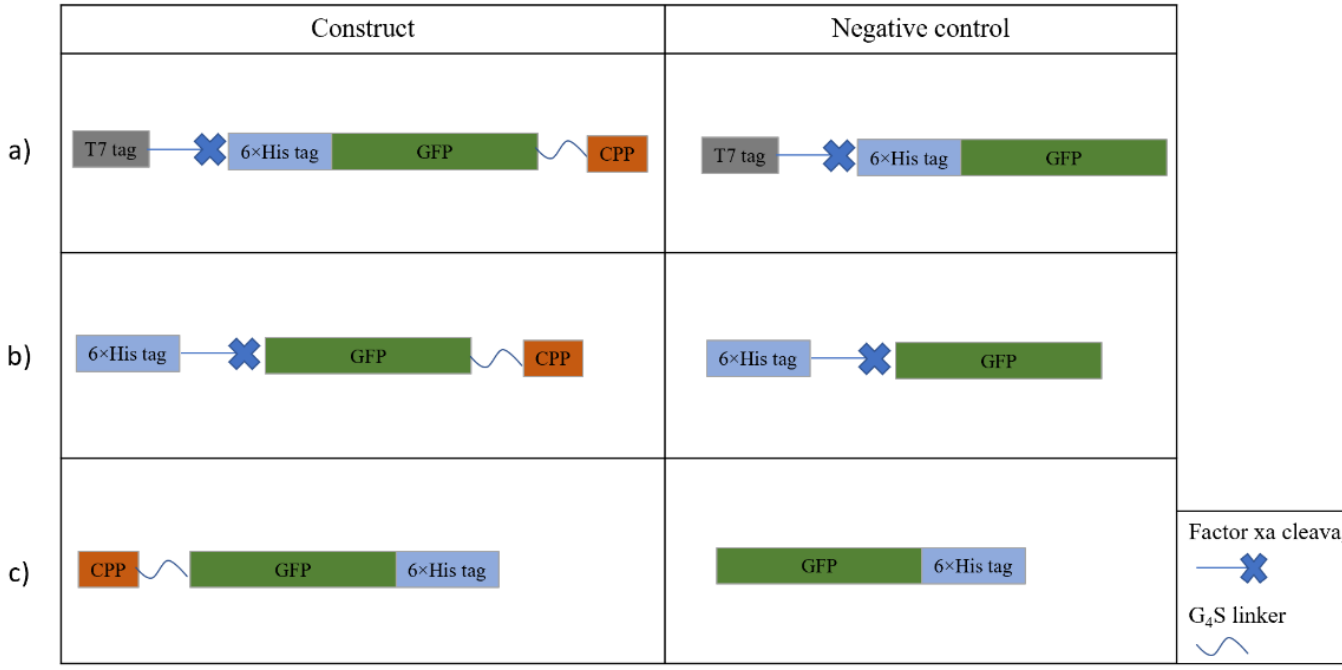

Figure 3.2 Schematic overview of designed recombinant proteins with the GFP attached at the N- and C-terminus of the CPP. the T7 tag was included to increase expression level, and the factor Xa cleavage site was included to remove the T7 tag or 6×His tag if required. There is a sequence coding for G_4S between GFP and the CPP to provide more flexibility and increase the translocation23.

The bacteriophage T7 epitope (T7 tag) consists of 11 amino acids (MASMTGGQQMG), and, when located upstream of the target gene, it can increase the recombinant protein expression[37]. It can also be used as an affinity tag for purification and detection of the target protein. A hexahistidine tag (HHHHHH; 6×His tag) was fused to the protein for purification and detection purposes[38]. The advantage of the 6×His tag is that it rarely impacts protein function due to its small size and low charge[37]. A factor Xa cleavage site with the sequence I(E/D)GR was incorporated to allow removal of the T7 tag for downstream applications using factor Xa protease, which recognizes the sequence and cleaves after the arginine residue[38]. We designed

unique restriction enzyme sites at both ends of each component, so they are exchangeable with one another or with different components for future studies. A glycine-serine linker peptide (G_4S) was included to improve expression, since it was previously found to be effective in increasing the protein expression and helping with translocation into *C. albicans* cells23.

The pET system used in this study is one of the most popular systems for cloning recombinant proteins, and it does not express the target recombinant protein until it is induced by an appropriate agent, which is very helpful when working with CPPs that might be toxic to the cells. The expression strain is BL21(DE3) *E. coli*, which contains the T7 RNA polymerase gene. This gene is regulated by lacUV5 promoter, and once induced with, IPTG,), it will promote the transcription and expression of the target protein[39].

After expressing the GFP-G_4S-MPG construct, we ran a Western blot to compare its expression with the MPG-G_4S-GFP construct, which was shown previously to have a high level of expression32 (Figure 3.3a). We did not detect the 6×His tag in the GFP-G_4S-MPG; however, the previously produced MPG-G_4S-GFP was detected by the antibody in the same blot. This suggested that either the GFP-G_4S-MPG fusion protein was not expressed by the cells or the 6×His tag at its N-terminus was not present or not detectable in this construct (Figure 3.3a). When pelleting the MPG-G_4S-GFP and GFP-G_4S-MPG by centrifugation, we noticed that the pellet of the MPG-G_4S-GFP culture was green, but the GFP-G_4S-MPG was not green,

so we assumed that the issue was expression of the construct. To help select for a colony capable of expressing the construct, we modified our protocol to screen the transformed cells for the expression of the GFP before assessing the expression of the whole construct with Western blotting. We identified multiple GFP-expressing clones containing the GFP-G_4S-MPG plasmid and performed Western blotting to detect 6×His tag and GFP (Figures 3.3b,c). Presence of GFP was confirmed by Western blotting, but the 6×His tag was still not detectable. One possible reason for the inability to detect the 6×His tag is that the protein may have been truncated due to the proteolytic cleavage in recombinant protein production.

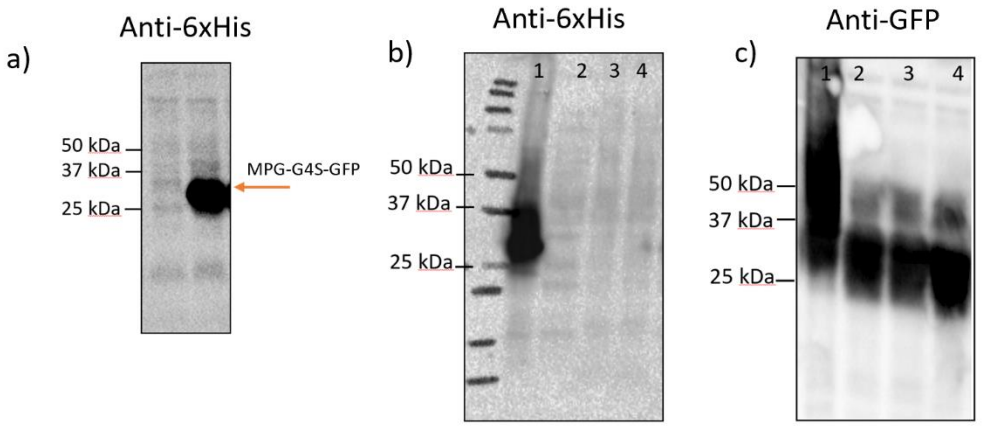

Figure 3.3 Expression of the GFP-G_4S-MPG. (a) Blot stained with anti-6xHis antibody with only MPG-G4S-GFP construct detected. (b,c) Comparing MPG-G_4S-GFP in Lane 1 with three different green clones of GFP-G_4S-MPG picked from an LB plate containing IPTG (Lanes 2-4). Blot stained with anti-6xHis (b) and anti-GFP (c).

To determine if this result was specific for MPG or more general, we built two plasmids in which the MPG was replaced with the peptides MAP and pVEC. We obtained the

same results observed with the MPG peptide: no 6×His tag was detected, but GFP was detected (Figure 3.3a). We noticed two close bands for GPF-G_4S-MPG that might be due to degradation of the peptide, while the GFP-G_4S-MAP and GFP-G_4S-pVEC seem to be intact with only one band being detected by anti-GFP (Figure 3.4a). This can be used to compare the stability of three peptides, indicating that pVEC and MAP are more stable than MPG which is consistent with the data found for pVEC in the literature[40].We do not know why the 6×His tag was not detected at the N-terminus of the GFP-G_4S-MPG. We decided to add a T7 epitope tag to the N-terminus of the construct to help the detection of 6×His tag by using the properties of T7 epitope tag which helps increasing expression of recombinant proteins38 (Figure 3.2a). After addition of the T7 tag, the Western blot results showed some traces of the presence of 6×His tag in the T7-GFP-G_4S-MPG (Figure 3.4b). However, the levels were still not comparable to the MPG-G_4S-GFP construct. On the other hand, the anti-GFP results were promising and showed the expression of GFP in all the constructs (Figure 3.4b). Based on the results from the Western blot, we assumed that 6×His is not detectable by the Western blot, and we decided to test whether we could purify the construct by IMAC using Ni-charged resins. The purification was successful, showing that the 6×His tag was present and accessible for attachment to the Ni-charged resins. We will discuss the purification results in detail in the Section 3.2.

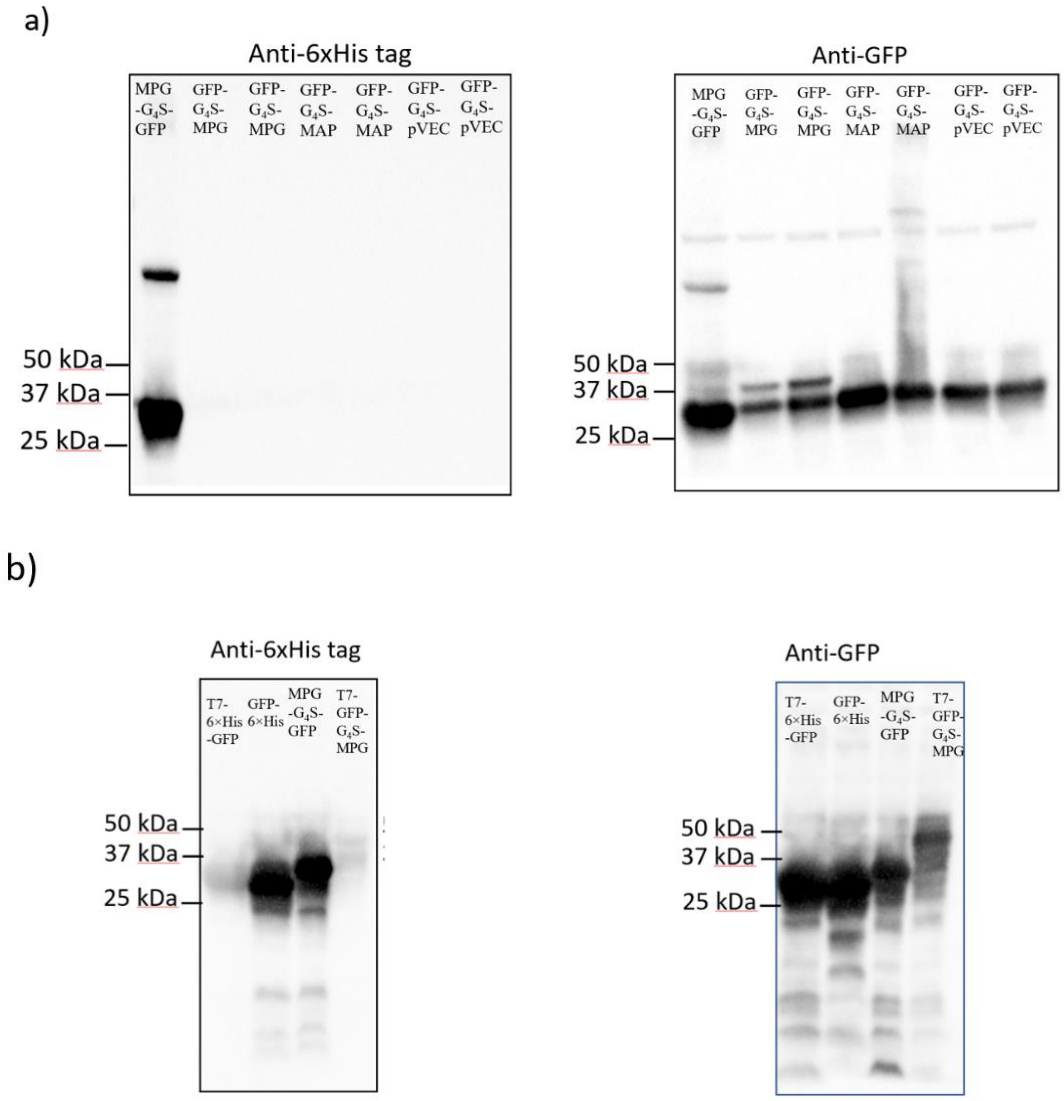

Figure 3.4 Expression of GFP-G$_4$S-MAP, GFP-G$_4$S-pVEC, and T7-GFP-G$_4$S-MPG. (a) Expression of plasmids containing GFP-G$_4$S-CPP compared to MPG-G$_4$S-GFP with anti-6xHis and anti-GFP antibodies. (b) Expression of GFP-G$_4$S-MPG is increased when T7-tag was fused to the N-terminus of the construct.

The expression of recombinant proteins containing CPPs can be challenging32, like having unacceptable degradation or expression of protein in inclusion body. In the case of T7-GFP-G$_4$S-MPG, we expected expression to be straightforward, based on the

previous high expression level of MPG-G_4S-GFP32. GFP is well produced and well folded in *E. coli*42 and can function as a soluble expression partner, so moving it to the N-terminus was expected to improve expression. Our observation that the expression of both constructs, the GFP-G_4S-MPG and T7- GFP-G_4S-MPG was lower than the MPG-G_4S-GFP, highlights the difficulties in expressing CPP fusions and the lack of a defined protocol for their expression. More research to understand the exact behavior of CPPs when they are fused to other proteins is needed.

3.3 Purification and protein characterization

In this part of the work our main purpose was to purify the recombinant proteins and prepare them for the translocation study.

3.3.1 Purification results

Our proteins contained the 6×His tag, which has affinity to metal ions like Ni^{2+}, Zn^{2+}, and Cu^{2+}39. The proteins were purified using Ni-charged IMAC resins under native (non-reducing) conditions. We collected samples from wash and elution steps and analyzed them on an SDS-PAGE gel to see what sizes of protein each sample contained and determine the purity of the desired protein construct (Figure 3.5). The SDS-PAGE was analyzed with densitometry to determine the purity of the proteins (Table 3.1). All proteins showed almost 99% purity, except for T7-GFP-G_4S-MPG. T7-GFP-G_4S-MPG had two bands near the expected size of the protein. These two bands were seen in the

Western blots, as well (Figure 3.4a), and we assume that the lower band is a degradation product of T7-GFP-G_4S-MPG.

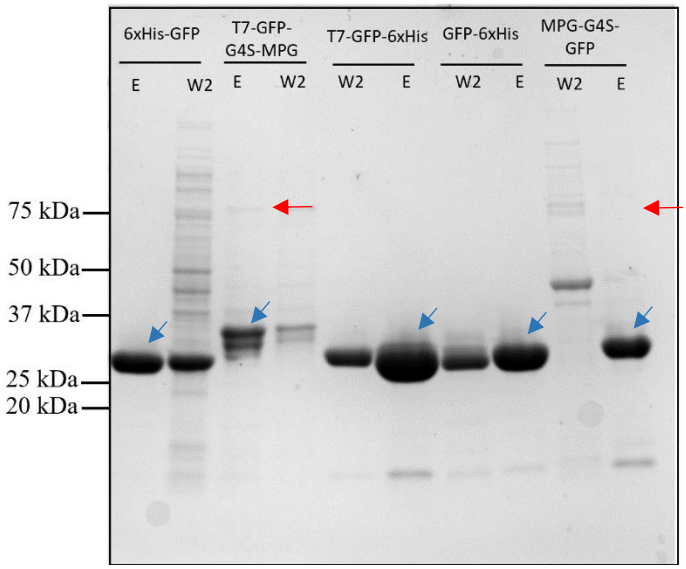

Figure 3.5 Representative SDS-PAGE result for all the constructs used in this study. The eluate (E) and the wash (W2) were separated by SDS-PAGE and stained with Coomassie stain. The lowest purity belongs to GFP-G_4S-MPG. The blue arrows show the desired size in the eluate of each sample. The red arrows show shared impurity between T7-GFP-G_4S-MPG and MPG-G_4S-GFP.

Table 3.1 The purity of the constructs after one step of IMAC purification.

Protein construct	**Purity**
T7-GFP-G_4S-MPG	52%
T7-6×His-GFP	~99%
T7-GFP-6×His	~99%
MPG-G_4S-GFP	~99%
GFP-6×His	~99%

When washing with 10 mM imidazole to remove loosely bound proteins, we noticed that the samples collected from this wash (W2) were green for most proteins, indicating the early elution of GFP. After analysis of the wash samples with SDS-PAGE, we observed that a portion of target protein was the most abundant protein eluted in the wash for most proteins, with the exception being MPG-G_4S-GFP where other impurities were eluted (Figure 3.5). For the other samples, the washing solution did not remove a substantial amount of impurity but did remove the desired protein. Because of this, for the rest of our experiments, we eliminated washing with 10 mM imidazole for every protein except for MPG-G4S-GFP.

3.3.2 SEC results

SEC was performed on T7-GFP-G_4S-MPG, MPG-G_4S-GFP, and T7-6×His-GFP to visualize the presence of soluble aggregates in the purified protein samples. T7-6×His-GFP showed only one peak at around a volume of 15 mL (Figure 3.6a), which, according to the column calibration, is at the volume we expect for the elution of a protein the size of T7-6×His-GFP (30 kDa). These results suggest T7-6×His-GFP does not form soluble aggregates. On the other hand, T7-GFP-G_4S-MPG (33 kDa) (Figure 3.6b) and MPG-G_4S-GFP (30 kDa) (Figure 3.6c) both showed a peak at a volume of 9.2 mL, in addition to the primary peak at the size expected for monomeric versions of these constructs. The peak at 9.2 mL represents a size of around 700 kDa, which is very large compared to the size of both constructs. The fusion of peptides to GFP can lead to aggregate formation43, and, since we did not observe a peak eluting at the same volume when analyzing T7-6×His-GFP, this peak could be indicating the formation of

very large soluble aggregates containing nearly 30 monomeric proteins. We compared the relative area under the aggregate peak to the relative area under the peak representing the desired proteins (T7-GFP-G_4S-MPG and MPG-G_4S-GFP), and we found a higher relative amount of aggregated protein in the T7-GFP-G_4S-MPG protein sample (13% aggregated) than in the MPG-G_4S-GFP protein sample (2% aggregated).This suggests that the relative position of the CPP and GFP influences aggregation, and T7-GFP-G_4S-MPG is more aggregation-prone than MPG-G_4S-GFP.

a) T7-6×His-GFP

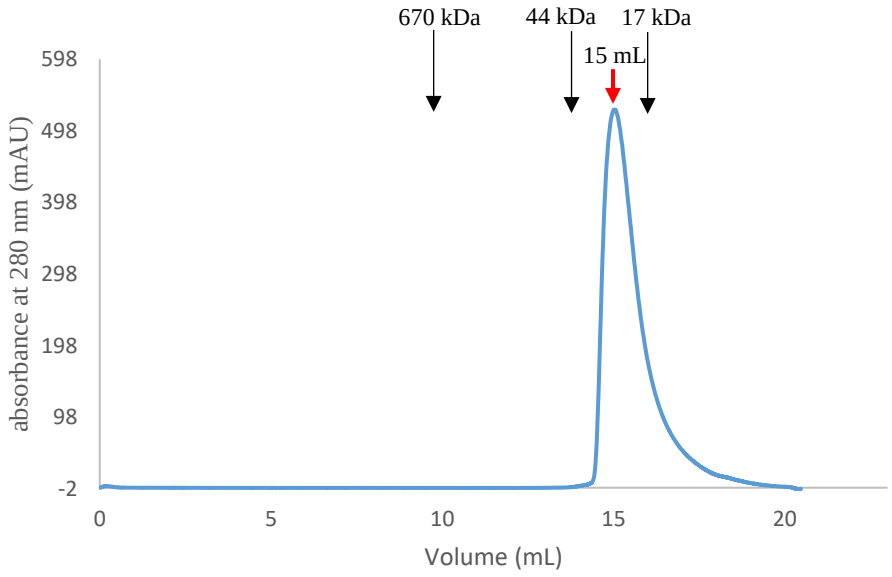

b) T7-GFP-G_4S-MPG

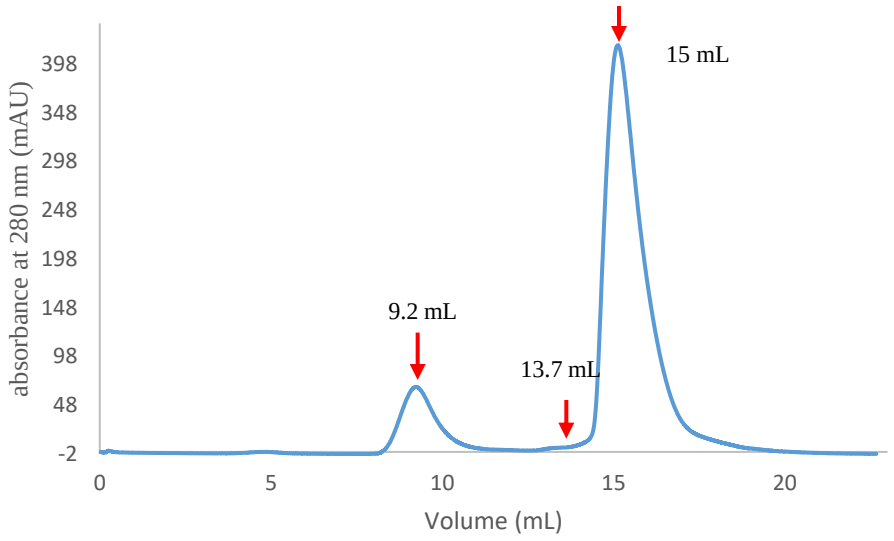

c) MPG-G_4S-GFP

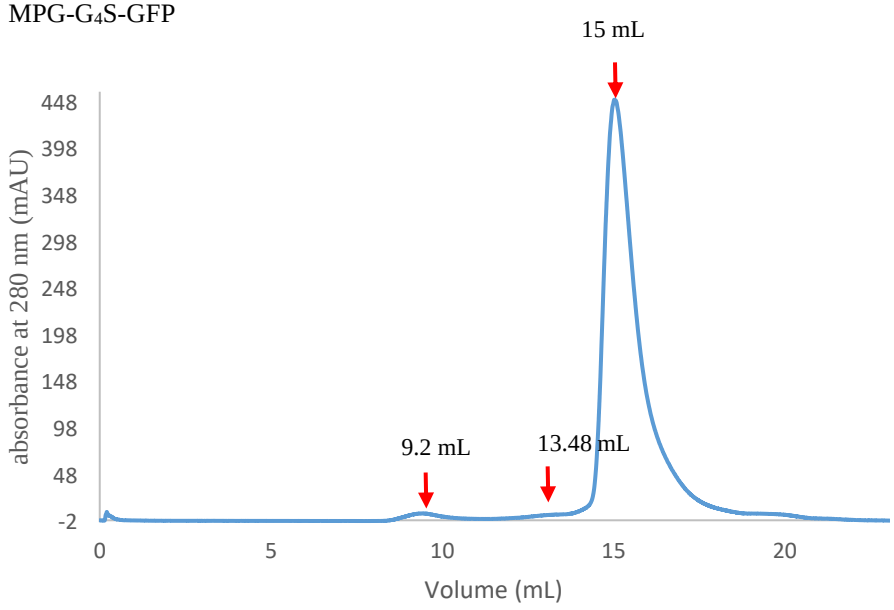

Figure 3.6 SEC results for (a) T7-6×His-GFP, (b) T7-GFP-G_4S-MPG, and (c) MPG-G_4S-GFP. The purified proteins were concentrated to 200 mM total protein concentration (purity of construct was not considered) and run on an SEC column to look for soluble aggregate formation. Protein concentration eluted in the volume fractions is proportional to UV absorbance at 280 nm. The red arrows indicate the volume where the peaks appear. The black arrows mark the elution volume of the standards and the corresponding size of proteins eluted at these volumes.

Just before the peak corresponding to monomeric protein for T7-GFP-G_4S-MPG and MPG-G_4S-GFP (at a volume of around 15 mL), we observed a slight increase of absorbance at a volume of 13.7 mL. This increase was consistently repeated in all our experiments with T7-GFP-G_4S-MPG and MPG-G_4S-GFP but not with T7-6×His-GFP. This peak falls between 158 kDa and 44 kDa (red arrows on the Figures 3.4b and 3.4c) and could represent an impurity in the purified protein samples that corresponds to a protein with a size of about 75 kDa. The impurity can be seen on the SDS-PAGE results for T7-GFP-G_4S-MPG and MPG-G_4S-GFP (Figure 3.5), but the band is faint for MGP-G_4S-GFP. Another possibility for this peak is that it indicates some smaller soluble aggregates in these samples, with each aggregate containing around 3 monomers.

The results from SEC, indicating that our proteins are forming aggregates, is consistent with the results from a previous study on MPG-G_4S-GFP with dynamic light scattering (DLS)29. We do not know what effect aggregation has on the interaction of the MPG with GFP and the constructs with *C. albicans* cells or their translocation into cells, but this would be an interesting topic for further research.

3.4 Effect of T7 tag on the translocation of cargo without CPP

As discussed in Section 3.2, we found the T7 tag improved the expression of the T7-GFP-G_4S-MPG construct compared to the construct without the T7 tag. To determine whether the T7 tag affects translocation into *C. albicans* cells, we compared translocation of the purified proteins T7-GFP-6×His and GFP-6×His by detecting the

presence of GFP in cells following incubation with the proteins for 1, 8, and 24 h. Following washing and treating with trypsin to remove protein attached to the surface of the cells, we performed flow cytometry to measure the fluorescence of the cells to detect intracellular GFP. To quantify the membrane permeabilization, we added PI to each sample immediately before analysis with flow cytometry. GFP-6×His has been tested for translocation previously in our lab, and it showed a low, but measurable, level of translocation into *C. albicans*, even though it contains no CPP 30.

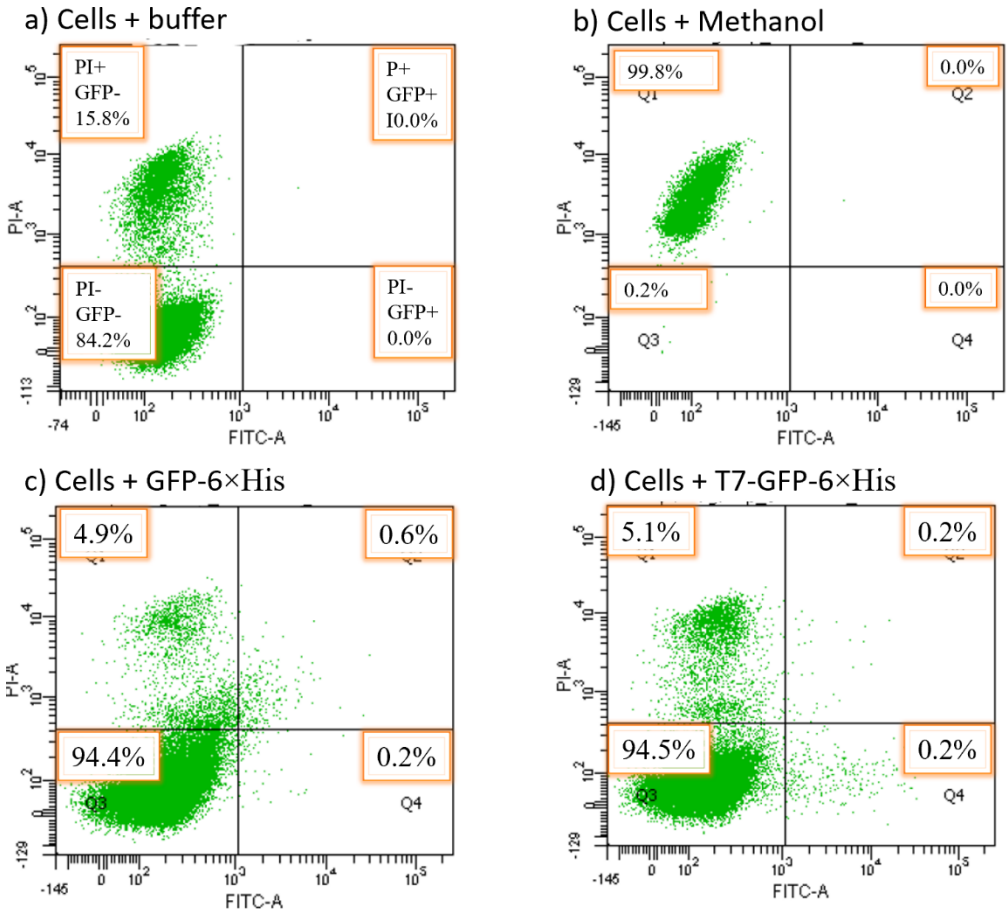

Figure 3.7 Translocation of T7-GFP-6×His and GFP-6×His into *C. albicans* cells. Flow cytometry was used to measure translocation of cargo into *C. albicans* cells. Multiple replicates of the experiment were done, and these data are representative of samples after incubation for 24 h with cells. PI was added

to the sample prior to analysis with flow cytometry to determine the membrane permeabilization. The dot plots are for (a) cells incubated with buffer only, (b) cells incubated with methanol, (c) cells incubated with GFP-6×His, and (d) cells incubated with T7-GFP-6×His. The quadrant Q1 represents cells that do not contain GFP (GFP-) but have PI translocated in the cells (PI+), Q2 represents cells with both GFP+ and PI+ (GFP+/PI+), Q3 contains the intact cells with no PI and no GFP inside (GFP-/PI-), and Q4 represents cells with GFP+ only (GFP+/PI-). The number in each quadrant represents the percentage of cells falling in that quadrant, and each dot in the plots represents a single cell.

Flow cytometry was used to measure the GFP fluorescence and PI fluorescence of each cell (Figure 3.7). To quantify the translocation of the T7-GFP-6×His and GFP-6×His, we used the data from the dot plots to determine the percentage of all cells in each sample containing GFP. The percentage of GFP-positive cells includes the cells from quadrant Q4 (GFP+/PI-) and quadrant Q2 (GFP+/PI-) in the dot plots (Figure 3.7).

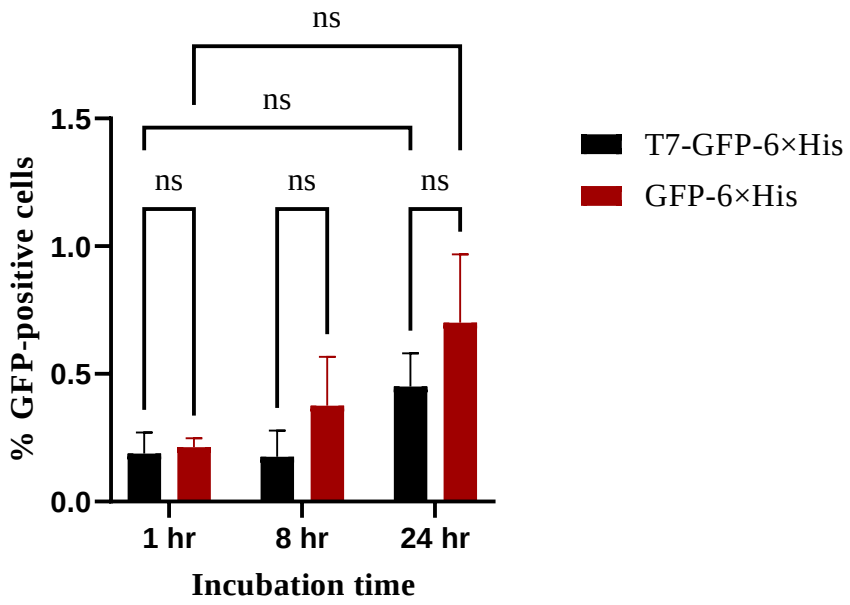

Figure 3.8 Impact of T7 tag at the N-terminus of GFP (without CPP) on the translocation into *C. albicans*. The two constructs were incubated with *C. albicans* for 1 h, 8 h, and 24 h, and the percentage

of cells containing GFP fluorescence was determined by flow cytometry. The experiment included 6 replicates (three biological replicates each containing two technical replicates). The error bars represent the standard error of the mean. Brackets indicate the statistical significance of pairs of samples (ns: not significant).

As shown in Figure 3.8, the difference in translocation between the constructs with and without the T7 tag was not statistically significant, so we concluded that the presence of the T7 tag does not affect translocation. With that in mind, subsequent experiments with the CPP at the C-terminus of GFP included the T7 tag in the protein fusion constructs, since the T7 tag improved the expression of the construct containing the CPP (Section 3.1). Our protein fusion design does include a factor Xa cleavage site to remove the T7 tag, if desired for future applications.

3.4 Effect of CPP attachment location on the translocation of cargo

There are two orientations possible for the fusion of CPP to the cargo: CPP-cargo or cargo-CPP. Each of these orientations might affect the interaction between the CPP and cargo, as well as the interaction of the whole construct with the cell membrane. We designed fusions with both orientations to determine the effect of orientation on translocation. The constructs MPG-G_4S-GFP and T7-GFP-G_4S-MPG, along with negative controls lacking a CPP, were incubated with *C. albicans* for 1, 8, and 24 h and analyzed with flow cytometry.

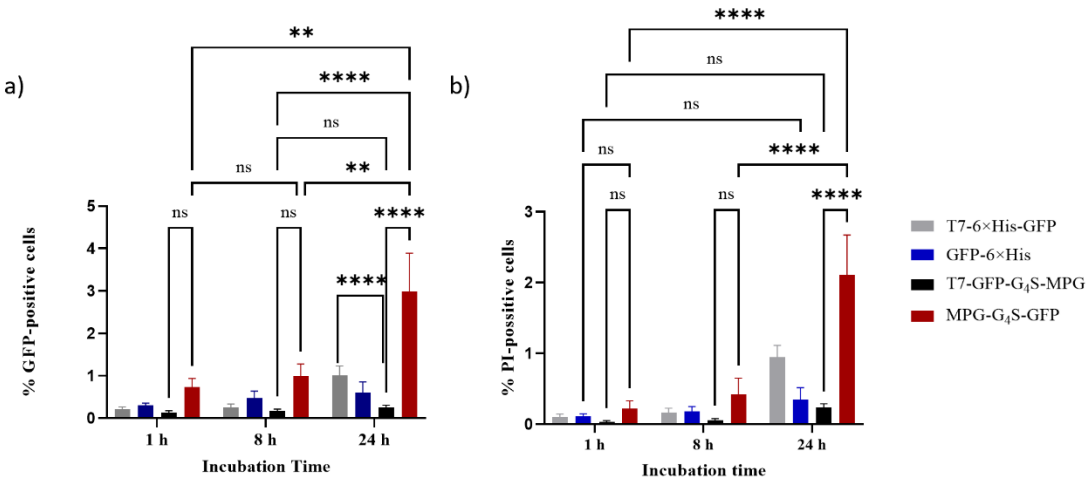

Figure 3.9 Translocation of GFP into *C. albicans* cells. Flow cytometry data are graphed for the translocation of MPG-G_4S-GFP, T7-GFP-G_4S-MPG, 6×His-GFP, and GFP-6×His into cells following incubation with the cells for the indicated time. (a) The percentage of GFP-positive cells represents the mean of cells that are PI+/GFP+ and PI-/GFP+ (flow cytometry dot plot quadrants Q2 and Q4 in Figure 3.7) for a total of 8 replicates. (b) The percentage of PI-positive cells represents cells that are PI+/GFP+ only (Q2 in Figure 3.7) of the same 8 replicates represented in (a). The error bars represent standard error of the mean. Asterisks on the brackets indicate the significance level for the indicated sets of data (ns= not significant, *=P<0.05, ** =P<0.01; ***= P<0.001, and ****= P<0.0001).

Based on the data in Figure 3.9.a, both negative control GFP constructs without a CPP (T7-6×His-GFP and GFP-6×His) translocate into the *C. albicans* cells; however, their translocation is not significant, and this is consistent with previous analyses in our lab on the translocation of GFP constructs lacking a CPP into *C. albicans*23,29.

MPG-G_4S-GFP does translocate into *C. albicans* cells at levels above the negative control, and we observed a significantly higher translocation of the MPG-G_4S-GFP into the cells at 24 h compared with 1 h and 8 h of incubation with cells, which was observed

in the previous study in our lab, as well29. The translocation of MPG-G_4S-GFP following incubation with cells for 24 h varied widely in our experiments, ranging from 0.9 to 8.6 % of cells having GFP translocated inside in the data plotted in Figure 3.9. Once during our experiments, we observed a translocation of 65%, increasing the overall average translocation of MPG-G_4S-GFP to almost 10% (see Appendix A, Figure A.2); however, since this high level of translocation was an order of magnitude higher than our other results and not repeated in our experiments, we did not include this set of data in Figure 3.9 or in associated statistical analyses. Although we observed high translocation with MPG-G_4S-GFP only once in our experiments, similarly high levels of translocation of MPG-G_4S-GFP have previously been observed in our lab[30]. With that in mind, the results from the translocation assay support the hypothesis that MPG-G_4S-GFP does carry large cargos inside the cells, but the translocation level can vary widely, and more research is required to obtain a high and reproducible translocation of MPG-G_4S-MPG into the *C. albicans* cells.

When changing the position of the cargo from the C-terminus of the CPP (MPG-G_4S-GFP) to its N-terminus (T7-GFP-G_4S-MPG), we noticed a significant reduction in translocation (Figure 3.9a). In fact, no significant translocation of the T7-GFP-G_4S-MPG compared to the control T7-6×His-GFP was observed after 1 and 8 h of incubation, and the negative control was significantly higher than T7-GFP-G_4S-MPG after incubation for 24 h (Figure 3.9a). This observation is supported by the simulation study on the translocation of MPG without cargo, which was done by Dr. Jeffery Klauda's group31. The simulation results indicate that MPG inserts into the cell

membrane with its N-terminal end initiating the insertion29,31. This is consistent with the observation of MPG-G_4S-GFP translocating into the cells at levels significantly higher than T7-GFP-G_4S-MPG. In the construct T7-GFP-G_4S-MPG, the part of CPP that is responsible for interaction with the cell membrane is attached to GFP and may not be able to initiate the membrane insertion required for translocation.

In addition to considering the translocation of GFP, we also considered the permeability of the cells by evaluating uptake of PI (Figure 3.9b), which only enters cells with damaged membranes, in the cells containing GFP (GFP+/PI+) (Figure 3.9b). During all the experiments, we observed both intact cells containing GFP (GFP+, PI-) and permeabilized cells with translocated GFP (GFP+, PI). The permeabilization of the cells may be a result of pore formation by the MPG and the cells failing to repair the pore. It may also be due to cell death, unrelated to translocation of the CPPs, since we observed 15% of dead cells that were permeable to PI in the flow cytometry results from cells incubating in buffer only (Figure 3.7a). Based on these data, we cannot conclude that translocation of MPG-G_4S-GFP into the cells leads to membrane disruption and subsequently cell death, but it is possible that they have some toxicity toward the cell, which would be beneficial for antifungal applications of our work.

3.6 The effect of protein concentration on translocation

To see if increasing the concentration of protein results in enhanced translocation for MPG-G_4S-GFP, we compared two protein concentrations during translocation: 100 μM and 400 μM. (These concentrations take the purity of the protein construct into

consideration; see Section 2.7.) We incubated the constructs with the *C. albicans* cells for 1 and 24 h before performing flow cytometry.

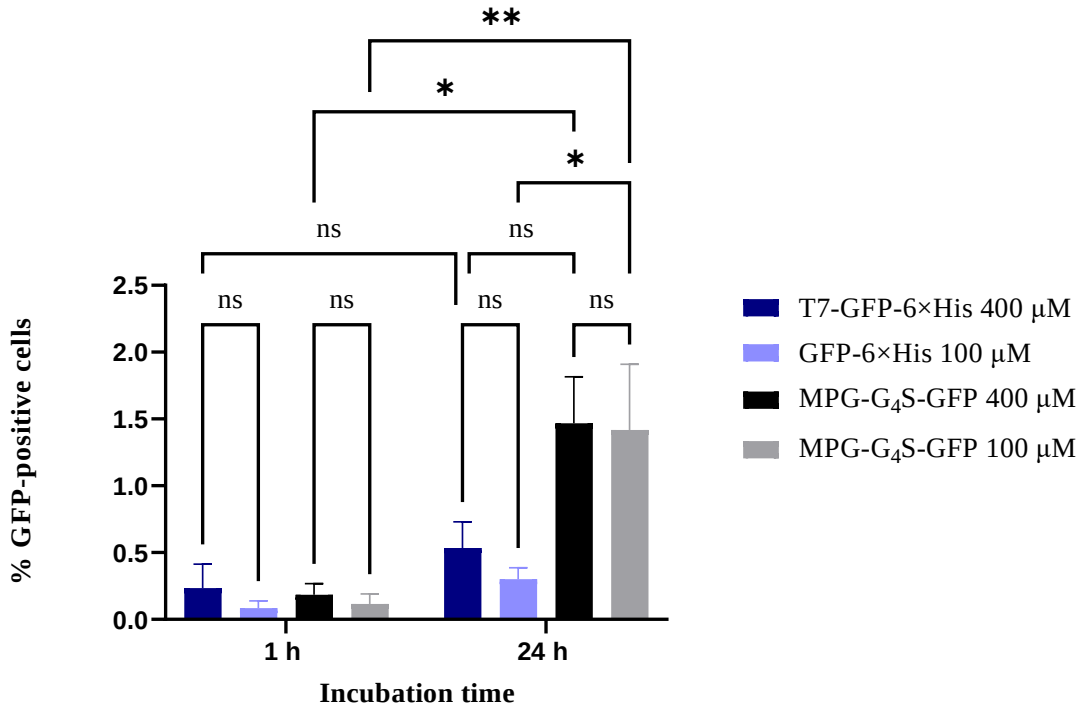

Figure 3.10 Effect of protein concentration on the translocation into fungal cells. Flow cytometry data from 3 replicates that were carried out on 3 different days using 3 different batches of purified proteins are plotted. The percentage of GFP-positive cells considers both GFP+/PI+ and GFP+/ PI- cells. The error bars represent the standard error of the mean.

Increasing the protein concentration from 100 µM to 400 µM had no statistically significant effect on the translocation of the constructs into *C. albicans* cells (Figure 3.10). We observed that both concentrations show significantly higher translocation at 24 h compared to 1h. However, the level of significance for the proteins at 100 µM is higher (Figure 3.10). These results are consistent with the previous study in our lab on

CPPs, which found that increasing concentration above 100 μM does not help MPG to translocate better29.

Chapter 4: Conclusion and future work

4.1 Conclusion

In this study, we evaluated the effect of the position of GFP, which represents a cargo attached to a CPP, on the ability of MPG to translocate and carry the cargo inside *C. albicans* cells. We found that the position of the cargo has a significant effect on the translocation of the whole construct, with GFP fused to the C-terminus of the MPG being the optimum position for the cargo. When the GFP was fused to the N-terminus, little to no translocation was detected, likely because the peptide requires the N-terminal residues for interaction with the cell membrane. We learned that CPPs can carry a large cargo like GFP into *C. albicans* cells, but our results with the MPG peptide shows a large variation in the translocation rate of the CPP-cargo fusion, indicating that, despite the ability of this CPP to take the cargo into the *C. albicans* cells, more work is needed to achieve robust translocation results.

4.2 Future work

The variations observed in the translocation of MPG in this thesis and previous work in our lab[27,29] emphasize the need for more research on improving translocation efficacy of CPP-fusion constructs. Below, we describe possible alternative CPPs and CPP formats, along with a suggested study to better understand degradation products produced during recombinant production of T7-GFP-G_4S-MPG.

4.2.1 Substitution of MPG with pVEC and SynB

In the previous studies in our lab, pVEC, MAP, and SynB showed that they can carry a fluorescent label into almost 100% of *C. albicans* cells27, but they have not been tested for larger cargoes like GFP. MAP and pVEC did show toxicity towards *C. albicans* cell, but a previous study has shown that the toxicity can be reduced by reduction in the hydrophobicity of the peptide26. One possible future experiment for improving delivery of cargo to the *C. albicans* cells is changing MPG to pVEC, SynB, and/or MAP to evaluate their translocation into the cells. Based on the toxicity data, manipulation of MAP and pVEC via rational design might be required if low levels of toxicity are desirable26. According to previous studies, if the cargo is attached to the appropriate end of the CPPs, we may see much higher translocation with these CPPs than what we observed with MPG.

4.2.2 Cyclization of MPG

Cyclization of CPPs has been reported to help the delivery of enhanced GFP (eGFP) directly into the cytosol of the mammalian cells[27]. The addition of two cysteine residues at appropriate locations of the MPG will promote the formation of a disulfide bond between the cysteines and create a cyclized MPC (cMPG) (Figure 4.1). Considering the results from simulations and experiments showing that the N-terminus of MPG plays a major role in the penetration of the peptide across the cell membrane, we need to consider the design in a way that the N-terminal end is free. Cyclization of peptides through disulfide bonds needs at least 4 amino acids between the two cysteine

residues45. In order to keep the N-terminal end free, we need to add a free cysteine residue at the C-terminus and one in the middle of the MPG. Since we do not know how many amino acids are required for internalization of the constructs at the N-terminus, we propose the creation of an initial library of cMPGs through rational design by a cysteine residue at various locations of the MPG (Table 4.1). The charged residues are located at the C-terminal end (KKKRKV) and a sequence of amino acids (WSQP) links hydrophobic and hydrophilic domains, so our initial library cyclizes the charged residues including the linker (cMPG1). Based on the results with the initial library, additional locations for cysteines could be evaluated to find the optimal location.

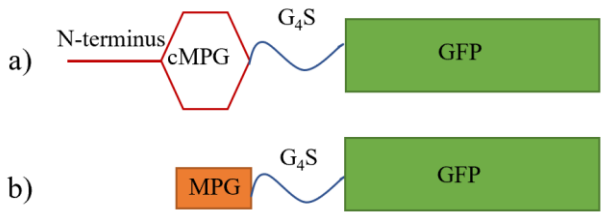

Figure 4.1 Schematic representation of (a) cMPG-G$_4$S-GFP and (b) MPG-G$_4$S-GFP

Table 4.1 Suggested library of cMPGs

Sample	Sequence
cMPG1	GALFLGFLGAAGSTMGACWSQPKKKRKVC
cMPG2	GALFLGFLGAAGSTMCGAWSQPKKKRKVC
cMPG3	GALFLGFLGAAGSCTMGAWSQPKKKRKVC
cMPG4	GALFLGFLGAACGSTMGAWSQPKKKRKVC
cMPG5	GALFLGFLGCAAGSTMGAWSQPKKKRKVC
cMPG6	GALFLGFCLGAAGSTMGAWSQPKKKRKVC
cMPG7	GALFLCGFLGAAGSTMGAWSQPKKKRKVC

cMPG8	GALCFLGFLGAAGSTMGAWSQPKKKRKVC
cMPG9	GCALFLGFLGAAGSTMGAWSQPKKKRKVC

Simulations can be incorporated to choose the most promising cMPGs from the library, and then, after expression and purification of the desired cMPG-G_4S-GFP proteins, we can compare translocation into *C. albicans* cells with the linear MPG-G_4S-GFP experimentally to see whether cyclization will improve the translocation efficiency and reproducibility. Additionally, the cyclization of the CPP might increase the stability of the peptide by limiting the possible conformations.

4.2.3 Identification of degradation product

As was discussed in Sections 3.1 and 3.2, we observed a degradation product on the SDS-PAGE gel in the T7-GFP-G_4S-MPG purified sample (Figure 3.5). Although we considered the purity of the T7-GFP-G_4S-MPG in our experiments (assuming the larger band represented full-length protein), the presence of the degradation product suggests the construct is not completely proteolytically stable, introducing the possibility that even what we thought was full-length protein may not have all the amino acids for MPG. The characterization of both the "full-length" protein and degradation product by mass spectrometry will give validity to the results of this study. We observed little to no level of translocation of the T7-GFP-G_4S-MPG into the cells but knowing that this construct is unstable makes us consider that the CPP was truncated at the end.

Appendix A

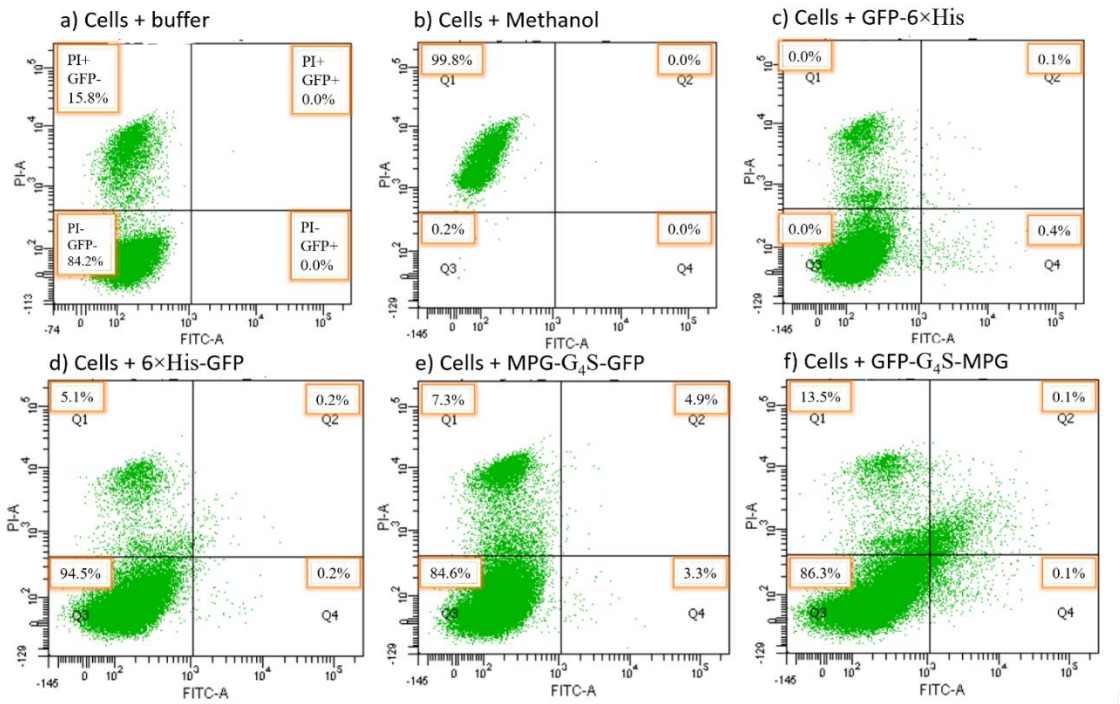

Figure A.1 Flow cytometry data for one replicate after 24 h incubation with *C. albicans*. Flow cytometry was used to get the data for translocation of cargo into the *C. albicans* cells. Multiple replicates of the experiment have been done, and these data are representative of samples after incubation for 24 h with cells. PI was added to the sample prior to analysis with flow cytometry to determine the membrane permeabilization. The dot plots are for (a) cells incubated with buffer only, (b) cells incubated with methanol, (c) cells incubated with GFP-6×His, (d) cells incubated with 6×His-GFP, (e) cells incubated with MPG-G_4S-GFP, and (f) cells incubated with T7-GFP-G_4S-MPG. The quadrant Q1 represents cells that do not contain GFP (GFP-) but have PI translocated in the cells (PI+), Q2 represents cells with both GFP+ and PI+ (GFP+/PI+), Q3 contains the intact cell with no PI and no GFP inside (GFP-/PI-), and Q4 represents cells with GFP+ only (GFP+/PI-). The number in each quadrant represents the percentage of cells falling in that quadrant, and each dot in the plots represents a single cell.

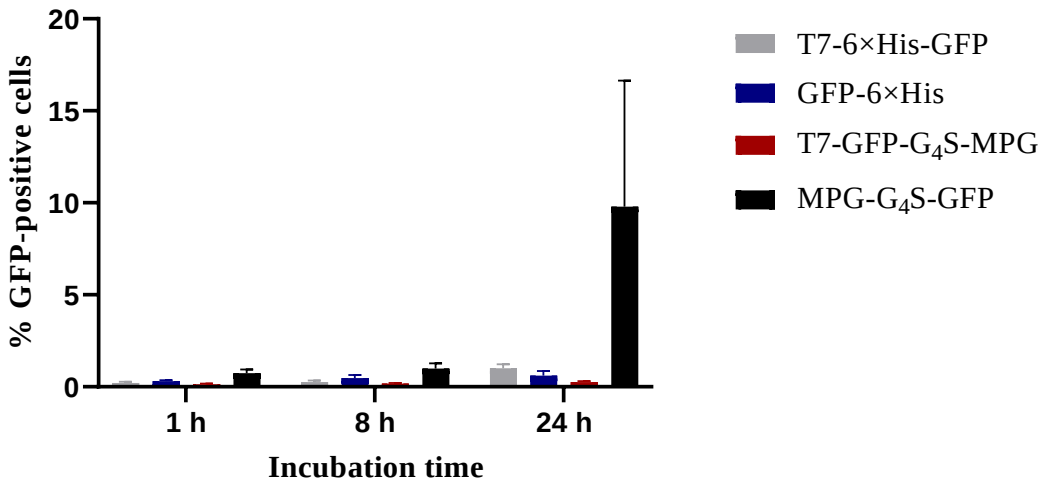

Figure A.2 The average translocation of constructs into *C. albicans* cells including replicate with very high translocation. Flow cytometry data are graphed for MPG-G_4S-GFP, T7-GFP-G_4S-MPG, 6×His-GFP, and GFP-6×His. Following incubation with the cells for the indicated time, the percentage of GFP-positive cells represents the mean of cells that are PI+/GFP+ and PI-/GFP+ (flow cytometry dot plot quadrants Q2 and Q4 in Figure A2) for a total of 9 replicates. The replicate showing a high level of translocation is included in this graph. The error bars represent standard error of mean.

Appendix B

Table B. 1. Statistical analysis for impact of T7 tag at the N-terminus of GFP (without CPP) on the translocation into *C. albicans* (Figure 3.8)

Tukey's multiple comparisons test	Mean difference	95% CI of difference	Summary	Adjusted P-value
1 hr: T7-GFP-6×His vs. 1 hr: GFP-6×His	-0.025	-0.6071 to 0.5571	ns	>0.9999
1 hr: T7-GFP-6×His vs. 8 hr: T7-GFP-6×His	0.0125	-0.5696 to 0.5946	ns	>0.9999
1 hr: T7-GFP-6×His vs. 8 hr: GFP-6×His	-0.1875	-0.7696 to 0.3946	ns	0.9274
1 hr: T7-GFP-6×His vs. 24 hr: T7-GFP-6×His	-0.2625	-0.8446 to 0.3196	ns	0.7578
1 hr: T7-GFP-6×His vs. 24 hr: GFP-6×His	-0.5125	-1.095 to 0.06959	ns	0.1128
1 hr: GFP-6×His vs. 8 hr: T7-GFP-6×His	0.0375	-0.5446 to 0.6196	ns	>0.9999
1 hr: GFP-6×His vs. 8 hr: GFP-6×His	-0.1625	-0.7446 to 0.4196	ns	0.9595
1 hr: GFP-6×His vs. 24 hr: T7-GFP-6×His	-0.2375	-0.8196 to 0.3446	ns	0.8256
1 hr: GFP-6×His vs. 24 hr: GFP-6×His	-0.4875	-1.070 to 0.09459	ns	0.1473
8 hr: T7-GFP-6×His vs. 8 hr: GFP-6×His	-0.2	-0.7821 to 0.3821	ns	0.9066
8 hr: T7-GFP-6×His vs. 24 hr: T7-GFP-6×His	-0.275	-0.8571 to 0.3071	ns	0.7207
8 hr: T7-GFP-6×His vs. 24 hr: GFP-6×His	-0.525	-1.107 to 0.05709	ns	0.0981
8 hr: GFP-6×His vs. 24 hr: T7-GFP-6×His	-0.075	-0.6571 to 0.5071	ns	0.9988
8 hr: GFP-6×His vs. 24 hr: GFP-6×His	-0.325	-0.9071 to 0.2571	ns	0.5606
24 hr: T7-GFP-6×His vs. 24 hr: GFP-6×His	-0.25	-0.8321 to 0.3321	ns	0.7929

Table B. 2. Statistical analysis for translocation of GFP into *C. albicans* cells. T. The percentage of GFP-positive cells represents the mean of cells that are PI+/GFP+ and PI-/GFP+. (Figure 3.9a).

Tukey's multiple comparisons test	Mean difference	95% CI of difference	Summary	Adjusted P-value
1 h: T7-6×His-GFP vs. 1 h: GFP-6×His	-0.08889	-1.403 to 1.225	ns	>0.9999
1 h: T7-6×His-GFP vs. 1 h: T7-GFP-G$_4$S-MPG	0.07778	-1.237 to 1.392	ns	>0.9999
1 h: T7-6×His-GFP vs. 1 h: MPG-G$_4$S-GFP	-0.5222	-1.837 to 0.7921	ns	0.9728
1 h: T7-6×His-GFP vs. 8 h: T7-6×His-GFP	-0.04444	-1.359 to 1.270	ns	>0.9999
1 h: T7-6×His-GFP vs. 8 h: GFP-6×His	-0.2667	-1.581 to 1.048	ns	>0.9999
1 h: T7-6×His-GFP vs. 8 h: T7-GFP-G$_4$S-MPG	0.04444	-1.270 to 1.359	ns	>0.9999
1 h: T7-6×His-GFP vs. 8 h: MPG-G$_4$S-GFP	-0.7778	-2.092 to 0.5365	ns	0.7034
1 h: T7-6×His-GFP vs. 24 h: T7-6×His-GFP	-0.8	-2.114 to 0.5143	ns	0.6655
1 h: T7-6×His-GFP vs. 24 h: GFP-6×His	-0.4	-1.714 to 0.9143	ns	0.9969
1 h: T7-6×His-GFP vs. 24 h: T7-GFP-G$_4$S-MPG	-0.04444	-1.359 to 1.270	ns	>0.9999
1 h: T7-6×His-GFP vs. 24 h: MPG-G$_4$S-GFP	-2.776	-4.131 to -1.422	****	<0.0001
1 h: GFP-6×His vs. 1 h: T7-GFP-G$_4$S-MPG	0.1667	-1.148 to 1.481	ns	>0.9999
1 h: GFP-6×His vs. 1 h: MPG-G$_4$S-GFP	-0.4333	-1.748 to 0.8810	ns	0.9938
1 h: GFP-6×His vs. 8 h: T7-6×His-GFP	0.04444	-1.270 to 1.359	ns	>0.9999
1 h: GFP-6×His vs. 8 h: GFP-6×His	-0.1778	-1.492 to 1.137	ns	>0.9999
1 h: GFP-6×His vs. 8 h: T7-GFP-G$_4$S-MPG	0.1333	-1.181 to 1.448	ns	>0.9999
1 h: GFP-6×His vs. 8 h: MPG-G$_4$S-GFP	-0.6889	-2.003 to 0.6254	ns	0.8367
1 h: GFP-6×His vs. 24 h: T7-6×His-GFP	-0.7111	-2.025 to 0.6032	ns	0.8068
1 h: GFP-6×His vs. 24 h: GFP-6×His	-0.3111	-1.625 to 1.003	ns	0.9997
1 h: GFP-6×His vs. 24 h: T7-GFP-G$_4$S-MPG	0.04444	-1.270 to 1.359	ns	>0.9999
1 h: GFP-6×His vs. 24 h: MPG-G$_4$S-GFP	-2.688	-4.042 to -1.333	****	<0.0001
1 h: T7-GFP-G$_4$S-MPG vs. 1 h: MPG-G$_4$S-GFP	-0.6	-1.914 to 0.7143	ns	0.9284
1 h: T7-GFP-G$_4$S-MPG vs. 8 h: T7-6×His-GFP	-0.1222	-1.437 to 1.192	ns	>0.9999
1 h: T7-GFP-G$_4$S-MPG vs. 8 h: GFP-6×His	-0.3444	-1.659 to 0.9699	ns	0.9992
1 h: T7-GFP-G$_4$S-MPG vs. 8 h: T7-GFP-G$_4$S-MPG	-0.03333	-1.348 to 1.281	ns	>0.9999
1 h: T7-GFP-G$_4$S-MPG vs. 8 h: MPG-G$_4$S-GFP	-0.8556	-2.170 to 0.4588	ns	0.567
1 h: T7-GFP-G$_4$S-MPG vs. 24 h: T7-6×His-GFP	-0.8778	-2.192 to 0.4365	ns	0.5271

1 h: T7-GFP-G$_4$S-MPG vs. 24 h: GFP-6×His	-0.4778	-1.792 to 0.8365	ns	0.9862
1 h: T7-GFP-G$_4$S-MPG vs. 24 h: T7-GFP-G$_4$S-MPG	-0.1222	-1.437 to 1.192	ns	>0.9999
1 h: T7-GFP-G$_4$S-MPG vs. 24 h: MPG-G$_4$S-GFP	-2.854	-4.209 to -1.499	****	<0.0001
1 h: MPG-G$_4$S-GFP vs. 8 h: T7-6×His-GFP	0.4778	-0.8365 to 1.792	ns	0.9862
1 h: MPG-G$_4$S-GFP vs. 8 h: GFP-6×His	0.2556	-1.059 to 1.570	ns	>0.9999
1 h: MPG-G$_4$S-GFP vs. 8 h: T7-GFP-G$_4$S-MPG	0.5667	-0.7477 to 1.881	ns	0.9512
1 h: MPG-G$_4$S-GFP vs. 8 h: MPG-G$_4$S-GFP	-0.2556	-1.570 to 1.059	ns	>0.9999
1 h: MPG-G$_4$S-GFP vs. 24 h: T7-6×His-GFP	-0.2778	-1.592 to 1.037	ns	0.9999
1 h: MPG-G$_4$S-GFP vs. 24 h: GFP-6×His	0.1222	-1.192 to 1.437	ns	>0.9999
1 h: MPG-G$_4$S-GFP vs. 24 h: T7-GFP-G$_4$S-MPG	0.4778	-0.8365 to 1.792	ns	0.9862
1 h: MPG-G$_4$S-GFP vs. 24 h: MPG-G$_4$S-GFP	-2.254	-3.609 to -0.8994	****	<0.0001
8 h: T7-6×His-GFP vs. 8 h: GFP-6×His	-0.2222	-1.537 to 1.092	ns	>0.9999
8 h: T7-6×His-GFP vs. 8 h: T7-GFP-G$_4$S-MPG	0.08889	-1.225 to 1.403	ns	>0.9999
8 h: T7-6×His-GFP vs. 8 h: MPG-G$_4$S-GFP	-0.7333	-2.048 to 0.5810	ns	0.7744
8 h: T7-6×His-GFP vs. 24 h: T7-6×His-GFP	-0.7556	-2.070 to 0.5588	ns	0.7399
8 h: T7-6×His-GFP vs. 24 h: GFP-6×His	-0.3556	-1.670 to 0.9588	ns	0.9989
8 h: T7-6×His-GFP vs. 24 h: T7-GFP-G$_4$S-MPG	2.78E-16	-1.314 to 1.314	ns	>0.9999
8 h: T7-6×His-GFP vs. 24 h: MPG-G$_4$S-GFP	-2.732	-4.087 to -1.377	****	<0.0001
8 h: GFP-6×His vs. 8 h: T7-GFP-G$_4$S-MPG	0.3111	-1.003 to 1.625	ns	0.9997
8 h: GFP-6×His vs. 8 h: MPG-G$_4$S-GFP	-0.5111	-1.825 to 0.8032	ns	0.9768
8 h: GFP-6×His vs. 24 h: T7-6×His-GFP	-0.5333	-1.848 to 0.7810	ns	0.9682
8 h: GFP-6×His vs. 24 h: GFP-6×His	-0.1333	-1.448 to 1.181	ns	>0.9999
8 h: GFP-6×His vs. 24 h: T7-GFP-G$_4$S-MPG	0.2222	-1.092 to 1.537	ns	>0.9999
8 h: GFP-6×His vs. 24 h: MPG-G$_4$S-GFP	-2.51	-3.864 to -1.155	****	<0.0001
8 h: T7-GFP-G$_4$S-MPG vs. 8 h: MPG-G$_4$S-GFP	-0.8222	-2.137 to 0.4921	ns	0.6265
8 h: T7-GFP-G$_4$S-MPG vs. 24 h: T7-6×His-GFP	-0.8444	-2.159 to 0.4699	ns	0.5869
8 h: T7-GFP-G$_4$S-MPG vs. 24 h: GFP-6×His	-0.4444	-1.759 to 0.8699	ns	0.9923
8 h: T7-GFP-G$_4$S-MPG vs. 24 h: T7-GFP-G$_4$S-MPG	-0.08889	-1.403 to 1.225	ns	>0.9999
8 h: T7-GFP-G$_4$S-MPG vs. 24 h: MPG-G$_4$S-GFP	-2.821	-4.176 to -1.466	****	<0.0001
8 h: MPG-G$_4$S-GFP vs. 24 h: T7-6×His-GFP	-0.02222	-1.337 to 1.292	ns	>0.9999

8 h: MPG-G$_4$S-GFP vs. 24 h: GFP-6×His	0.3778	-0.9365 to 1.692	ns	0.9981
8 h: MPG-G$_4$S-GFP vs. 24 h: T7-GFP-G$_4$S-MPG	0.7333	-0.5810 to 2.048	ns	0.7744
8 h: MPG-G$_4$S-GFP vs. 24 h: MPG-G$_4$S-GFP	-1.999	-3.353 to -0.6438	***	0.0002
24 h: T7-6×His-GFP vs. 24 h: GFP-6×His	0.4	-0.9143 to 1.714	ns	0.9969
24 h: T7-6×His-GFP vs. 24 h: T7-GFP-G$_4$S-MPG	0.7556	-0.5588 to 2.070	ns	0.7399
24 h: T7-6×His-GFP vs. 24 h: MPG-G$_4$S-GFP	-1.976	-3.331 to -0.6216	***	0.0002
24 h: GFP-6×His vs. 24 h: T7-GFP-G$_4$S-MPG	0.3556	-0.9588 to 1.670	ns	0.9989
24 h: GFP-6×His vs. 24 h: MPG-G$_4$S-GFP	-2.376	-3.731 to -1.022	****	<0.0001
24 h: T7-GFP-G$_4$S-MPG vs. 24 h: MPG-G$_4$S-GFP	-2.732	-4.087 to -1.377	****	<0.0001

Table B. 3. Statistical analysis for translocation of GFP into *C. albicans* cells. The percentage of PI-positive cells represents cells that are PI+/GFP+ only (Figure 3.9b)

Tukey's multiple comparisons test	Mean difference	95% CI of difference	Summary	Adjusted P-value
1 h: T7-6×His-GFP vs. 1 h: GFP-6×His	-0.01111	-0.9333 to 0.9110	ns	>0.9999
1 h: T7-6×His-GFP vs. 1 h: T7-GFP-G$_4$S-MPG	0.06667	-0.8555 to 0.9888	ns	>0.9999
1 h: T7-6×His-GFP vs. 1 h: MPG-G$_4$S-GFP	-0.1222	-1.044 to 0.7999	ns	>0.9999
1 h: T7-6×His-GFP vs. 8 h: T7-6×His-GFP	-0.06667	-0.9888 to 0.8555	ns	>0.9999
1 h: T7-6×His-GFP vs. 8 h: GFP-6×His	-0.07778	-0.9999 to 0.8444	ns	>0.9999
1 h: T7-6×His-GFP vs. 8 h: T7-GFP-G$_4$S-MPG	0.04444	-0.8777 to 0.9666	ns	>0.9999
1 h: T7-6×His-GFP vs. 8 h: MPG-G$_4$S-GFP	-0.3222	-1.244 to 0.5999	ns	0.99
1 h: T7-6×His-GFP vs. 24 h: T7-6×His-GFP	-0.8444	-1.767 to 0.07770	ns	0.1056
1 h: T7-6×His-GFP vs. 24 h: GFP-6×His	-0.2444	-1.167 to 0.6777	ns	0.9991
1 h: T7-6×His-GFP vs. 24 h: T7-GFP-G$_4$S-MPG	-0.1333	-1.055 to 0.7888	ns	>0.9999
1 h: T7-6×His-GFP vs. 24 h: MPG-G$_4$S-GFP	-2.011	-2.933 to -1.089	****	<0.0001
1 h: GFP-6×His vs. 1 h: T7-GFP-G$_4$S-MPG	0.07778	-0.8444 to 0.9999	ns	>0.9999
1 h: GFP-6×His vs. 1 h: MPG-G$_4$S-GFP	-0.1111	-1.033 to 0.8110	ns	>0.9999
1 h: GFP-6×His vs. 8 h: T7-6×His-GFP	-0.05556	-0.9777 to 0.8666	ns	>0.9999
1 h: GFP-6×His vs. 8 h: GFP-6×His	-0.06667	-0.9888 to 0.8555	ns	>0.9999
1 h: GFP-6×His vs. 8 h: T7-GFP-G$_4$S-MPG	0.05556	-0.8666 to 0.9777	ns	>0.9999
1 h: GFP-6×His vs. 8 h: MPG-G$_4$S-GFP	-0.3111	-1.233 to 0.6110	ns	0.9925
1 h: GFP-6×His vs. 24 h: T7-6×His-GFP	-0.8333	-1.755 to 0.08881	ns	0.1167
1 h: GFP-6×His vs. 24 h: GFP-6×His	-0.2333	-1.155 to 0.6888	ns	0.9994
1 h: GFP-6×His vs. 24 h: T7-GFP-G$_4$S-MPG	-0.1222	-1.044 to 0.7999	ns	>0.9999
1 h: GFP-6×His vs. 24 h: MPG-G$_4$S-GFP	-2	-2.922 to -1.078	****	<0.0001
1 h: T7-GFP-G$_4$S-MPG vs. 1 h: MPG-G$_4$S-GFP	-0.1889	-1.111 to 0.7333	ns	>0.9999
1 h: T7-GFP-G$_4$S-MPG vs. 8 h: T7-6×His-GFP	-0.1333	-1.055 to 0.7888	ns	>0.9999
1 h: T7-GFP-G$_4$S-MPG vs. 8 h: GFP-6×His	-0.1444	-1.067 to 0.7777	ns	>0.9999
1 h: T7-GFP-G$_4$S-MPG vs. 8 h: T7-GFP-G$_4$S-MPG	-0.02222	-0.9444 to 0.8999	ns	>0.9999

1 h: T7-GFP-G4S-MPG vs. 8 h: MPG-G4S-GFP	-0.3889	-1.311 to 0.5333	ns	0.9582
1 h: T7-GFP-G4S-MPG vs. 24 h: T7-6×His-GFP	-0.9111	-1.833 to 0.01103	ns	0.0559
1 h: T7-GFP-G4S-MPG vs. 24 h: GFP-6×His	-0.3111	-1.233 to 0.6110	ns	0.9925
1 h: T7-GFP-G4S-MPG vs. 24 h: T7-GFP-G4S-MPG	-0.2	-1.122 to 0.7221	ns	0.9999
1 h: T7-GFP-G4S-MPG vs. 24 h: MPG-G4S-GFP	-2.078	-3.000 to -1.156	****	<0.0001
1 h: MPG-G4S-GFP vs. 8 h: T7-6×His-GFP	0.05556	-0.8666 to 0.9777	ns	>0.9999
1 h: MPG-G4S-GFP vs. 8 h: GFP-6×His	0.04444	-0.8777 to 0.9666	ns	>0.9999
1 h: MPG-G4S-GFP vs. 8 h: T7-GFP-G4S-MPG	0.1667	-0.7555 to 1.089	ns	>0.9999
1 h: MPG-G4S-GFP vs. 8 h: MPG-G4S-GFP	-0.2	-1.122 to 0.7221	ns	0.9999
1 h: MPG-G4S-GFP vs. 24 h: T7-6×His-GFP	-0.7222	-1.644 to 0.1999	ns	0.2816
1 h: MPG-G4S-GFP vs. 24 h: GFP-6×His	-0.1222	-1.044 to 0.7999	ns	>0.9999
1 h: MPG-G4S-GFP vs. 24 h: T7-GFP-G4S-MPG	-0.01111	-0.9333 to 0.9110	ns	>0.9999
1 h: MPG-G4S-GFP vs. 24 h: MPG-G4S-GFP	-1.889	-2.811 to -0.9667	****	<0.0001
8 h: T7-6×His-GFP vs. 8 h: GFP-6×His	-0.01111	-0.9333 to 0.9110	ns	>0.9999
8 h: T7-6×His-GFP vs. 8 h: T7-GFP-G4S-MPG	0.1111	-0.8110 to 1.033	ns	>0.9999
8 h: T7-6×His-GFP vs. 8 h: MPG-G4S-GFP	-0.2556	-1.178 to 0.6666	ns	0.9987
8 h: T7-6×His-GFP vs. 24 h: T7-6×His-GFP	-0.7778	-1.700 to 0.1444	ns	0.1862
8 h: T7-6×His-GFP vs. 24 h: GFP-6×His	-0.1778	-1.100 to 0.7444	ns	>0.9999
8 h: T7-6×His-GFP vs. 24 h: T7-GFP-G4S-MPG	-0.06667	-0.9888 to 0.8555	ns	>0.9999
8 h: T7-6×His-GFP vs. 24 h: MPG-G4S-GFP	-1.944	-2.867 to -1.022	****	<0.0001
8 h: GFP-6×His vs. 8 h: T7-GFP-G4S-MPG	0.1222	-0.7999 to 1.044	ns	>0.9999
8 h: GFP-6×His vs. 8 h: MPG-G4S-GFP	-0.2444	-1.167 to 0.6777	ns	0.9991
8 h: GFP-6×His vs. 24 h: T7-6×His-GFP	-0.7667	-1.689 to 0.1555	ns	0.2031
8 h: GFP-6×His vs. 24 h: GFP-6×His	-0.1667	-1.089 to 0.7555	ns	>0.9999
8 h: GFP-6×His vs. 24 h: T7-GFP-G4S-MPG	-0.05556	-0.9777 to 0.8666	ns	>0.9999
8 h: GFP-6×His vs. 24 h: MPG-G4S-GFP	-1.933	-2.855 to -1.011	****	<0.0001
8 h: T7-GFP-G4S-MPG vs. 8 h: MPG-G4S-GFP	-0.3667	-1.289 to 0.5555	ns	0.9727

8 h: T7-GFP-G$_4$S-MPG vs. 24 h: T7-6×His-GFP	-0.8889	-1.811 to 0.03326	ns	0.0696
8 h: T7-GFP-G$_4$S-MPG vs. 24 h: GFP-6×His	-0.2889	-1.211 to 0.6333	ns	0.996
8 h: T7-GFP-G$_4$S-MPG vs. 24 h: T7-GFP-G$_4$S-MPG	-0.1778	-1.100 to 0.7444	ns	>0.9999
8 h: T7-GFP-G$_4$S-MPG vs. 24 h: MPG-G$_4$S-GFP	-2.056	-2.978 to -1.133	****	<0.0001
8 h: MPG-G$_4$S-GFP vs. 24 h: T7-6×His-GFP	-0.5222	-1.444 to 0.3999	ns	0.7579
8 h: MPG-G$_4$S-GFP vs. 24 h: GFP-6×His	0.07778	-0.8444 to 0.9999	ns	>0.9999
8 h: MPG-G$_4$S-GFP vs. 24 h: T7-GFP-G$_4$S-MPG	0.1889	-0.7333 to 1.111	ns	>0.9999
8 h: MPG-G$_4$S-GFP vs. 24 h: MPG-G$_4$S-GFP	-1.689	-2.611 to -0.7667	****	<0.0001
24 h: T7-6×His-GFP vs. 24 h: GFP-6×His	0.6	-0.3221 to 1.522	ns	0.568
24 h: T7-6×His-GFP vs. 24 h: T7-GFP-G$_4$S-MPG	0.7111	-0.2110 to 1.633	ns	0.3038
24 h: T7-6×His-GFP vs. 24 h: MPG-G$_4$S-GFP	-1.167	-2.089 to -0.2445	**	0.0029
24 h: GFP-6×His vs. 24 h: T7-GFP-G$_4$S-MPG	0.1111	-0.8110 to 1.033	ns	>0.9999
24 h: GFP-6×His vs. 24 h: MPG-G$_4$S-GFP	-1.767	-2.689 to -0.8445	****	<0.0001
24 h: T7-GFP-G$_4$S-MPG vs. 24 h: MPG-G$_4$S-GFP	-1.878	-2.800 to -0.9556	****	<0.0001

Table B. 4. Evaluating the effect of the protein concentration in the translocation into fungal cells.

(Figure 3.10)

Tukey's multiple comparisons test	Mean difference	95% CI of difference	Summary	Adjusted P-value
1 h: T7-GFP-6×His 400 µM vs. 1 h: GFP-6×His 100 µM	0.15	-0.9329 to 1.233	ns	0.9998
1 h: T7-GFP-6×His 400 µM vs. 1 h: MPG-G$_4$S-GFP 400 µM	0.05	-1.033 to 1.133	ns	>0.9999
1 h: T7-GFP-6×His 400 µM vs. 1 h: MPG-G$_4$S-GFP 100 µM	0.1167	-0.9663 to 1.200	ns	>0.9999
1 h: T7-GFP-6×His 400 µM vs. 24 h: T7-GFP-6×His 400 µM	-0.3	-1.383 to 0.7829	ns	0.9858
1 h: T7-GFP-6×His 400 µM vs. 24 h: GFP-6×His 100 µM	-0.06667	-1.150 to 1.016	ns	>0.9999
1 h: T7-GFP-6×His 400 µM vs. 24 h: MPG-G$_4$S-GFP 400 µM	-1.233	-2.316 to -0.1504	*	0.016
1 h: T7-GFP-6×His 400 µM vs. 24 h: MPG-G$_4$S-GFP 100 µM	-1.183	-2.266 to -0.1004	*	0.0237
1 h: GFP-6×His 100 µM vs. 1 h: MPG-G$_4$S-GFP 400 µM	-0.1	-1.183 to 0.9829	ns	>0.9999
1 h: GFP-6×His 100 µM vs. 1 h: MPG-G$_4$S-GFP 100 µM	-0.03333	-1.116 to 1.050	ns	>0.9999
1 h: GFP-6×His 100 µM vs. 24 h: T7-GFP-6×His 400 µM	-0.45	-1.533 to 0.6329	ns	0.8825
1 h: GFP-6×His 100 µM vs. 24 h: GFP-6×His 100 µM	-0.2167	-1.300 to 0.8663	ns	0.998
1 h: GFP-6×His 100 µM vs. 24 h: MPG-G$_4$S-GFP 400 µM	-1.383	-2.466 to -0.3004	**	0.0047
1 h: GFP-6×His 100 µM vs. 24 h: MPG-G$_4$S-GFP 100 µM	-1.333	-2.416 to -0.2504	**	0.0071
1 h: MPG-G$_4$S-GFP 400 µM vs. 1 h: MPG-G$_4$S-GFP 100 µM	0.06667	-1.016 to 1.150	ns	>0.9999
1 h: MPG-G$_4$S-GFP 400 µM vs. 24 h: T7-GFP-6×His 400 µM	-0.35	-1.433 to 0.7329	ns	0.9663
1 h: MPG-G$_4$S-GFP 400 µM vs. 24 h: GFP-6×His 100 µM	-0.1167	-1.200 to 0.9663	ns	>0.9999
1 h: MPG-G$_4$S-GFP 400 µM vs. 24 h: MPG-G$_4$S-GFP 400 µM	-1.283	-2.366 to -0.2004	*	0.0107
1 h: MPG-G$_4$S-GFP 400 µM vs. 24 h: MPG-G$_4$S-GFP 100 µM	-1.233	-2.316 to -0.1504	*	0.016
1 h: MPG-G$_4$S-GFP 100 µM vs. 24 h: T7-GFP-6×His 400 µM	-0.4167	-1.500 to 0.6663	ns	0.918
1 h: MPG-G$_4$S-GFP 100 µM vs. 24 h: GFP-6×His 100 µM	-0.1833	-1.266 to 0.8996	ns	0.9993
1 h: MPG-G$_4$S-GFP 100 µM vs. 24 h: MPG-G$_4$S-GFP 400 µM	-1.35	-2.433 to -0.2671	**	0.0062
1 h: MPG-G$_4$S-GFP 100 µM vs. 24 h: MPG-G$_4$S-GFP 100 µM	-1.3	-2.383 to -0.2171	**	0.0093
24 h: T7-GFP-6×His 400 µM vs. 24 h: GFP-6×His 100 µM	0.2333	-0.8496 to 1.316	ns	0.9969
24 h: T7-GFP-6×His 400 µM vs. 24 h: MPG-G$_4$S-GFP 400 µM	-0.9333	-2.016 to 0.1496	ns	0.136

24 h: T7-GFP-6×His 400 µM vs. 24 h: MPG-G_4S-GFP 100 µM	-0.8833	-1.966 to 0.1996	ns	0.1833
24 h: GFP-6×His 100 µM vs. 24 h: MPG-G_4S-GFP 400 µM	-1.167	-2.250 to -0.08373	*	0.0269
24 h: GFP-6×His 100 µM vs. 24 h: MPG-G_4S-GFP 100 µM	-1.117	-2.200 to -0.03373	*	0.0391
24 h: MPG-G_4S-GFP 400 µM vs. 24 h: MPG-G_4S-GFP 100 µM	0.05	-1.033 to 1.133	ns	>0.9999

Bibliography

(1) Richard A. Calderone; Cornelius J. Clancy. An Introduction to the Medically Important *Candida* species. In *Candida* and *Candidiasis;* American Society for Microbiology Press, 2011.

(2) Spampinato, C.; Leonardi, D. Candida Infections, Causes, Targets, and Resistance Mechanisms: Traditional and Alternative Antifungal Agents. BioMed Research International 2013, 2013. https://doi.org/10.1155/2013/204237.

(3) Nadeem, S. G.; Shafiq, A.; Hakim, S. T.; Anjum, Y.; U. Kazm, S. Effect of Growth Media, PH and Temperature on Yeast to Hyphal Transition in *Candida albicans*. Open Journal of Medical Microbiology 2013, *03* (03), 185–192. https://doi.org/10.4236/ojmm.2013.33028

(4) Flevari, A.; Theodorakopoulou, M.; Velegraki, A.; Armaganidis, A.; Dimopoulos, G. Treatment of Invasive *Candidiasis* in the Elderly: A Review. Clinical Interventions in Aging. September 7, 2013, pp 1199–1208. https://doi.org/10.2147/CIA.S39120.

(5) Pfaller, M. A.; Diekema, D. J. Epidemiology of Invasive *Candidiasis*: A Persistent Public Health Problem. Clinical Microbiology Reviews 2007, *20* (1), 133–163. https://doi.org/10.1128/CMR.00029-06.

(6) Li, L.; Sun, J.; Xia, S.; Tian, X.; Cheserek, M. J.; Le, G. Mechanism of Antifungal Activity of Antimicrobial Peptide APP, a Cell-Penetrating Peptide Derivative, against *Candida albicans*: Intracellular DNA Binding and Cell Cycle Arrest. Applied Microbiology and Biotechnology 2016, 100 (7), 3245–3253. https://doi.org/10.1007/s00253-015-7265-y.

(7) Mayer, F. L.; Wilson, D.; Hube, B. *Candida albicans* Pathogenicity Mechanisms. Virulence 2013, *4* (2), 119–128. https://doi.org/10.4161/viru.22913.

(8) Whaley, S. G.; Berkow, E. L.; Rybak, J. M.; Nishimoto, A. T.; Barker, K. S.; Rogers, P. D. Azole Antifungal Resistance in *Candida albicans* and Emerging Non-*albicans Candida* Species. Frontiers in Microbiology. Frontiers Media S.A. January 12, 2017. https://doi.org/10.3389/fmicb.2016.02173.

(9) Wiederhold, N. P. Antifungal Resistance: Current Trends and Future Strategies to Combat. Infection and Drug Resistance 2017, 10, 249–259. https://doi.org/10.2147/IDR.S124918.

(10) Leitner, T. L. Uptake of an Amphipathic CPP, MPG, as a Delivery System for MicroRNAs in 3T3-L1 Cells, Graz, 2021

(11) Cooper, G. M. The Cell: A Molecular Approach, 2nd ed.; Sinauer Associates: Sunderland, 2000

(12) Copolovici, D. M.; Langel, K.; Eriste, E.; Langel, Ü. Cell-Penetrating Peptides: Design, Synthesis, and Applications. ACS

Nano 2014, *8* (3), 1972–1994. https://doi.org/10.1021/nn4057269.
(13) Ziegler, A. Thermodynamic Studies and Binding Mechanisms of Cell-Penetrating Peptides with Lipids and Glycosaminoglycans. Advanced Drug Delivery Reviews 2008, 60 (4–5), 580–597. https://doi.org/10.1016/j.addr.2007.10.005.
(14) Guidotti, G.; Brambilla, L.; Rossi, D. Cell-Penetrating Peptides: From Basic Research to Clinics. Trends in Pharmacological Sciences. Elsevier Ltd April 1, 2017, pp 406–424. https://doi.org/10.1016/j.tips.2017.01.003.
(15) Koren, E.; Torchilin, V. P. Cell-Penetrating Peptides: Breaking through to the other side. Trends in Molecular Medicine 2012, 18 (7), 385–393. https://doi.org/10.1016/j.molmed.2012.04.012.
(16) Gräslund, A.; Madani, F.; Lindberg, S.; Langel, Ü.; Futaki, S. Mechanisms of Cellular Uptake of Cell-Penetrating Peptides. Journal of Biophysics 2011, 2011. https://doi.org/10.1155/2011/414729.
(17) Donaldson, J. G.; Porat-Shliom, N.; Cohen, L. A. Clathrin-Independent Endocytosis: A Unique Platform for Cell Signaling and PM Remodeling. Cellular Signaling 2009, 21 (1), 1–6. https://doi.org/10.1016/j.cellsig.2008.06.020.
(18) Gong, Z.; Ikonomova, S. P.; Karlsson, A. J. Secondary Structure of Cell-Penetrating Peptides during Interaction with Fungal Cells. Protein Science 2018, 27 (3), 702–713. https://doi.org/10.1002/pro.3364.
(19) Wang, F.; Wang, Y.; Zhang, X.; Zhang, W.; Guo, S.; Jin, F. Recent Progress of Cell-Penetrating Peptides as New Carriers for Intracellular Cargo Delivery. Journal of Controlled Release 2014, 174 (1), 126–136. https://doi.org/10.1016/j.jconrel.2013.11.020.
(20) Wagstaff, K.; Jans, D. Protein Transduction: Cell Penetrating Peptides and Their Therapeutic Applications. Current Medicinal Chemistry 2006, 13 (12), 1371–1387. https://doi.org/10.2174/092986706776872871.
(21) Gong, Z.; Walls, M. T.; Karley, A. N.; Karlsson, A. J. Effect of a Flexible Linker on Recombinant Expression of Cell-Penetrating Peptide Fusion Proteins and Their Translocation into Fungal Cells. Molecular Biotechnology 2016, 58 (12), 838–849. https://doi.org/10.1007/s12033-016-9983-5.
(22) Kristensen, M.; Birch, D.; Nielsen, H. M. Applications and Challenges for Use of Cell-Penetrating Peptides as Delivery Vectors for Peptide and Protein Cargos. International Journal of Molecular Sciences 2016, 17 (2). https://doi.org/10.3390/ijms17020185.
(23) Keller, A. A.; Mussbach, F.; Breitling, R.; Hemmerich, P.; Schaefer, B.; Lorkowski, S.; Reissmann, S. Relationships between Cargo, Cell Penetrating Peptides and Cell Type for

Uptake of Non-Covalent Complexes into Live Cells. Pharmaceuticals 2013, *6* (2), 184–203. https://doi.org/10.3390/ph6020184.
(24) Gong, Z.; Doolin, M. T.; Adhikari, S.; Stroka, K. M.; Karlsson, A. J. Role of Charge and Hydrophobicity in Translocation of Cell-Penetrating Peptides into *Candida albicans* Cells. AIChE Journal 2019, *65* (12). https://doi.org/10.1002/aic.16768.
(25) Gong, Z.; Karlsson, A. J. Translocation of Cell-Penetrating Peptides into *Candida* Fungal Pathogens. Protein Science 2017, 26 (9), 1714–1725. https://doi.org/10.1002/pro.3203.
(26) Patel, S. G.; Sayers, E. J.; He, L.; Narayan, R.; Williams, T. L.; Mills, E. M.; Allemann, R. K.; Luk, L. Y. P.; Jones, A. T.; Tsai, Y. H. Cell-Penetrating Peptide Sequence and Modification Dependent Uptake and Subcellular Distribution of Green Florescent Protein in Different Cell Lines. Scientific Reports 2019, 9 (1). https://doi.org/10.1038/s41598-019-42456-8.
(27) Adhikari, S. Translocation of Protein Cargo into *Candida albicans* Using Cell-Penetrating Peptides, PhD Thesis, university of Maryland, College Park, 2020.
(28) Adhikari, S. Translocation of Protein Cargo into *Candida albicans* Using Cell-Penetrating Peptides, PhD Thesis, university of Maryland, College Park, 2020.
(29) Adhikari S; Ghorbani M; Dura K; Klauda JB; Karlsson AJ. Translocation of CPP-Cargo Protein Fusion into Candida Albicans Cells and Designing for Enhanced Translocation with Simulations. In *Biophysical Society Annual Meeting*; Baltimore, 2019.
(30) Adhikari, S. Optimization of Recombinant Protein Expression for Cell-Penetrating Peptide Fusions to Protein Cargo, MS Thesis, university of Maryland, College Park, 2017.
(31) Rosano, G. L.; Ceccarelli, E. A. Recombinant Protein Expression in *Escherichia coli*: Advances and Challenges. Frontiers in Microbiology 2014, *5*. https://doi.org/10.3389/fmicb.2014.00172.
(32) PET System Manual. Novagen, Inc.1992.
(33) Yap Yen, P.; Trau, D. Yeast: Molecular and Cell Biology; 2019.
(34) Delagrave, S.; Hawtin, R. E.; Silva, C. M.; Yang, M. M.; Youvan, D. C. Red-Shifted Excitation Mutants of the Green Fluorescent Protein. Biotechnology (N Y) 1995, 13 (2), 151–154.
(35) Kong, J.; Wang, Y.; Qi, W.; Huang, M.; Su, R.; He, Z. Green Fluorescent Protein Inspired Fluorophores. Advances in Colloid and Interface Science 2020, *285*. https://doi.org/10.1016/j.cis.2020.102286.
(36) Simeoni, F.; Morris, M. C.; Heitz, F.; Divita, G. Insight into the Mechanism of the Peptide-Based Gene Delivery System MPG: Implications for Delivery of SiRNA into Mammalian Cells.

Nucleic Acids Research 2003, 31 (11), 2717–2724. https://doi.org/10.1093/nar/gkg385.
(37) Kimple, M. E.; Sondek, J. Overview of Affinity Tags for Protein Purification. Current protocols in protein science 2013, 73 (9.9.1-9.9.23). https://doi.org/10.1002/0471140864.ps0909s36.
(38) Gaberc-Porekar, V.; Menart, V. Potential for Using Histidine Tags in Purification of Proteins at Large Scale. Chemical Engineering and Technology 2005, 28 (11), 1306–1314. https://doi.org/10.1002/ceat.200500167.
(39) *Molecular Diagnosis of Infectious Diseases*.
(40) Holm, T.; Netzereab, S.; Hansen, M.; Langel, Ü.; Hällbrink, M. Uptake of Cell-Penetrating Peptides in Yeasts. FEBS Letters 2005, 579 (23), 5217–5222. https://doi.org/10.1016/j.febslet.2005.07.099.
(41) Su, W. W. Fluorescent Protein as Tools to Aid Protein Production. Microbial Cell Factories 2005, 4. https://doi.org/10.1186/1475-2859-4-12.
(42) Link, C. D.; Fonte, V.; Hiester, B.; Yerg, J.; Ferguson, J.; Csontos, S.; Silverman, M. A.; Stein, G. H. Conversion of Green Fluorescent Protein into a Toxic, Aggregation-Prone Protein by C-Terminal Addition of a Short Peptide. Journal of Biological Chemistry 2006, 281 (3), 1808–1816. https://doi.org/10.1074/jbc.M505581200.
(43) Kopple, K. D. Synthesis of Cyclic Peptides. Journal of Pharmaceutical Sciences 1972, 61 (9), 1345–1356.
(44) Sudbery, P.; Gow, N.; Berman, J. The Distinct Morphogenic States of *Candida albicans*. Trends in Microbiology 2004, 12 (7), 317–324. https://doi.org/10.1016/j.tim.2004.05.008.